

Article

# Source and Accumulation Analysis of Deviation during Multi-Level Assembly of an Aircraft Rear Fuselage Frame

Yaohui Zheng<sup>1</sup>, Xiaoyue Huang<sup>2,\*</sup>, Minghai Wang<sup>1</sup> and Pengcheng Hu<sup>2</sup><sup>1</sup> School of Mechanical and Electrical Engineering, Shenyang Aerospace University, Shenyang 110136, China<sup>2</sup> Key Laboratory of Fundamental Science for National Defence of Aeronautical Digital Manufacturing Process, Shenyang Aerospace University, Shenyang 110136, China

\* Correspondence: huangxiaoyue@stu.sau.edu.cn

**Abstract:** During the production process of aircraft assembly, weakly rigid parts are gradually assembled into rigid support structures in the aircraft skeleton through several assembly stations. The assembly deviations of this structure determine the quality of the aerodynamic shape of the aircraft. In this paper, we consider multiple sources of deviation (manufacturing deviation, fixture positioning deviation, assembly contact deviation) and investigate the interaction between these sources. Based on the state space approach, a state space equation is developed to reveal the transformation, accumulation and transfer of deviations in the multi-level assembly process (MAP) of weakly rigid parts, and a model is established to accurately simulate and predict the transfer of deviations in the MAP of weakly rigid parts. In this model, the part manufacturing and fixture positioning deviations in typical dimensional planes are regarded as rigid deviations, while the deviations in atypical dimensional planes are regarded as flexible deviations. A spatial triangle penetration detection algorithm based on part measurement point deviations is proposed, combined with the theory of linear elasticity, to describe the relationship between part deviations and assembly contact forces. An example analysis of the assembly process of an aircraft rear fuselage frame structure illustrates the validity of a multi-level assembly deviation transfer model for weakly rigid parts.

**Keywords:** multi-level assembly process; weakly rigid part; state space method; assembly contact force; rigid and compliant mixed deformation; numerical simulation analysis



**Citation:** Zheng, Y.; Huang, X.; Wang, M.; Hu, P. Source and Accumulation Analysis of Deviation during Multi-Level Assembly of an Aircraft Rear Fuselage Frame. *Appl. Sci.* **2023**, *13*, 9914. <https://doi.org/10.3390/app13179914>

Academic Editors: Marcin Graba and Stanisław Adamczak

Received: 14 August 2023

Revised: 26 August 2023

Accepted: 28 August 2023

Published: 1 September 2023



**Copyright:** © 2023 by the authors. Licensee MDPI, Basel, Switzerland. This article is an open access article distributed under the terms and conditions of the Creative Commons Attribution (CC BY) license (<https://creativecommons.org/licenses/by/4.0/>).

## 1. Introduction

The final overall quality of the support frame of an aircraft engine nacelle is generally determined by the machining accuracy of each wall panel and the assembly quality of multiple assembly stations. Currently, there are various research methods to assess multi-level assembly quality, the most representative of which are the influence coefficient method and the finite element method. Takezawa et al. [1] use measured data to predict the assembly deviation of automotive body-in-white parts with the help of linear regression equations in the numerical analysis, suggesting that the deviation of flexible sheet-metal thin-walled parts can no longer follow the traditional method of accumulating rigid deviations. Liu and Hu [2] discard the traditional methods of deviation analysis, such as the square root method and the Monte Carlo method, and propose using the finite element method to simulate the deviation variation of two-dimensional or three-dimensional sheet metal parts. Liu and Hu [3] consider the deviation characteristics of flexible parts and predict the box assembly deviation of flexible parts for the three most commonly used connection forms (lap, butt and corner) in part assembly, based on the small deformation assumption and finite element ideas, combining engineering structural models and statistical analysis methods. However, the studies described in the previous section are mostly limited to two-dimensional parts or consider only the rigid deviations of the parts. In the actual multi-station assembly process, flexible deviations of 3D parts are still one of the important

sources of deviations. In [4], a mixed-variable rigid-flexible modelling approach is proposed for sheet metal parts that are prone to flexible deformation during assembly. Based on a two-dimensional deviation flow model, the deviation transfer mechanism in each assembly step is investigated and the mathematical relationship between the total assembly deviation and the various sources of deviation is established accordingly. In [5], a process-oriented mathematical representation of the positioning datum system is proposed, containing detailed design parameters of the positioning datum system in the multi-station assembly (MSA), which creatively reveals the non-linear cumulative relationship between fixture deviations and errors in the positioning holes and slots of the part. In [6,7], both rigid and flexible deviations are considered and the impact of the deviations generated by each assembly process is analyzed and through the interaction between stations on the assembly quality by means of a transfer function mechanism.

Nowadays, in order to meet the increasingly stringent requirements for assembly quality in the aircraft and automotive industries, the issue of assembly contact during multi-level assembly has received more attention, and many scholars have achieved fruitful results in the field of predicting and controlling the contact state of assembly contact surfaces and the bearing forces in the assembly contact area. Dahlström and Lindkvist [8] improve on the influence coefficient method by means of a finite element analysis, consider the influence of contact forces on the assembly deviation of parts during the assembly process and propose a contact algorithm that can be implemented in the influence coefficient method. In [9,10], the technical characteristics of the aero-engine rotor assembly process are analyzed, with a focus on the detection method of coaxiality in assembly quality, and a solution for solving the parallel chain problem with deterministic deviation gravity is proposed. On the other hand, in [11,12], generalized elastic forces for anisotropic and orthotropic materials are derived from the point of view of material properties, taking into account material inhomogeneities and geometrical non-linearities, and force balance equations are used to investigate the deviation of thin-walled structural parts during assembly. Zhang et al. [13] illustrate the relationship between the position and orientation deviations of the part and the surface deviations of the part after assembly is completed. A deviation model for multi-part assembly is developed from the perspective of manufacturing errors, using the amount of deviation at the contact points as the controlling factor. Based on the finite element method, Xie et al. [14] propose an assembly method that considers the contact effects between parts and clamping elements, i.e., the enhanced dimensionality reduction method, for a highly non-linear part assembly system. In [15], the authors use a two-dimensional finite element model under linear elasticity to model the stress intensity factor in the static crack domain, analyze two typical fracture model problems and then use standard and multistage Monte Carlo methods combined with selective refiners to analyze several error tolerations, which significantly reduces the calculation cost.

It is worth noting that, with the development of the field of robotics engineering, many of the basic theories applied to robot dynamics systems have also been widely applied to the field of assembly deviation [16]. In [17], by introducing the concept of virtual joints, the Jacobian matrix was introduced into the tolerance transfer model for the first time, enriching the research gap in the field of multi-level assembly tolerance and the deviation control of parts. In [18], a novel method for the deviation analysis of three-dimensional parts is presented, using the Jacobian matrix model to describe the deviation of a partially parallel structure, and the deviation of a partially parallel structure consisting of a cylindrical contact pair and a planar contact pair is modelled through the combination of the parameters of the rotary quantities. In [19], the relative positioning method is combined with a quadratic planning technique to unify the calculation of series and parallel chains between parts in a complex assembly process. The use of discrete geometry based on point cloud technology instead of the traditional ideal surface model allows for the calculation of the cumulative assembly deviations in the Jacobi model in a simple way.

Among the many studies on multi-level assembly deviation theory, the stream of variation (SoV) theory is a very promising basic theory for deviation analysis and control. Liu and Hu [20] argued that product deviations in a production system would accumulate gradually and were the first to propose the theory of assembly deviation flow to investigate the mechanism of part assembly deviation propagation in a multi-level production system in terms of both the prediction and diagnosis of deviations. So far, a variety of deviation flow transmission and prediction theories have emerged, including the state space method, which is a classical approach in modern control theory. Using a “3-2-1” positioning scheme, Jin and Shi [21] first applied the state space method to the field of deviation transmission modelling, and the deviation transmission model established by the two scholars included key concepts, such as tool positioning error, part accumulation error and repositioning error. They also defined an observation equation to reveal the relationship between the observation vector and the state vector in a multi-level machining and manufacturing system. In [22], a deviation transfer and control model is proposed for multi-level linear dynamic assembly systems and different types of assembly joints by means of a state transformation model approach. In short, the introduction of the state space method presents a new way of solving the deviation transfer problem, allowing researchers to establish simple observation equations to predict and diagnose the transfer and accumulation of deviations in assembling complex assembly systems and to predict and react correctly to the accumulation of deviations in real time for each assembly step of the part. In [23], part deviations and fixture deviations are combined based on the influence coefficient method to study their propagation characteristics in multi-stage assembly systems, and a method to assess the propagation of dimensional changes in multi-station flexible transfer systems is proposed based on the linear elasticity theory and the state space method. In [24], it is pointed out that most assembly deviation prediction methods at the present stage focus on the product design and assembly stages, while ignoring the hazards caused by assembly deviations in the product service stage, and, therefore, a method is proposed for predicting assembly quality based on observable combined deviations.

However, the deviation transfer model based on the state space method is mostly limited to two-dimensional rigid parts and does not consider the flexible deformation of weakly rigid parts in three-dimensional space. In addition, the dimensionality of the observation equations will be greatly increased in the face of complex 3D assembly systems, and the observation vectors of the observation equations are difficult to unify. In [25], on the basis of the mainstream assembly quality prediction models, the comprehensive deformation of a part under the simultaneous influence of manufacturing errors and assembly loads was studied, not only considering the initial manufacturing errors of the part, but also using the flush coordinate transformation method to accurately establish a prediction model for the surface assembly accuracy of the part to be assembled. In [26], a non-linear state space is used to simulate the accumulation of deviations from one assembly station to the next by station with the objective of minimizing the sum of squares of the standard deviations of the critical products as well, and genetic algorithms are used to optimize the assembly quality problem in the multi-station assembly (MSA) of an automotive body. He et al. [27] investigate the impact of machine tool assembly deviations on tooling, consider components in an unassembled state, establish a method for pre-adjustment in the assembly design phase, and characterize the propagation of deviations during machine tool assembly by means of a state space approach.

On the basis of the above research, based on the linear elasticity theory and the state space method, a three-dimensional weakly rigid part multi-level assembly deviation transmission model is established for an assembly system containing multiple assembly stations, and a deviation state equation containing part rigidity and flexibility deviations, fixture deviations and assembly contact deviations is defined. Considering the problem of inconsistent observation vectors in the assembly system, a Jacobi-spinor method is used to represent the deviation propagation in three-dimensional space by means of the infinitesimal modelling of open kinematic chains in robot kinematics, and the part

coordinate system is correlated with the assembly (observation) coordinate system to obtain a unified observation vector and a concise equation of state. Finally, the computational procedure of the proposed method is presented with an aircraft engine nacelle as an example, and finite element simulation tests are carried out to verify the accuracy of the mathematical model of assembly deviation transmission.

## 2. Assembly Process and Assumptions for Weakly Rigid Parts

The assembly deviation of weakly rigid parts consists of part deviation, fixture positioning deviation and assembly contact deviation. In complex assembly systems containing multiple stations, the rigid and flexible deviations of the part are considered separately; weakly rigid parts are generally large parts with thin wall thicknesses of less than 1/10 of the typical overall structural dimensions, which are divided by size type into the typical structural dimension plane  $\sigma$  and the typical structural dimension normal plane  $\tau$  and the typical structural dimension projection plane  $\varphi$ . In the typical structural dimension, the deviation of the part mainly comes from its own manufacturing deviation and fixture positioning deviation. Without considering the manufacturing deviation of the part, the deviation of the part in the direction of typical structural dimensions can be considered rigid; however, in atypical structural dimensions, the flexible deformation of the part in the z-axis direction will be very obvious, and the flexible deformation mainly comes from the part deformation and fixture positioning deviation caused by machining stress, etc. As shown in Figure 1, a weakly rigid part has flexible deformation in the z-direction, with the xoy plane as  $\sigma$ , the xoz plane as  $\tau$  and the yoz plane as  $\varphi$ .

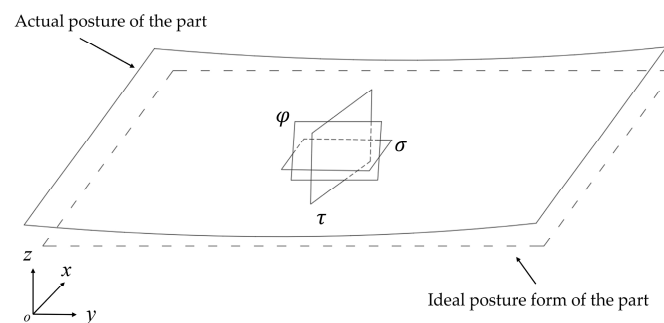


**Figure 1.** Flexible deformation of weakly rigid parts.

### 2.1. Fixture Layout for Weakly Rigid Parts

The positioning of weakly rigid parts in wall plate assembly is completed using special tooling, which is used to complete the positioning and clamping function of components called clamping elements or fixtures. Positioning is the process of obtaining the correct spatial position of the part on the tooling before assembly, and clamping is the process of fixing the part in a defined position by applying an external force. For arbitrary parts, the principle of six-point positioning is usually used, where the part to be clamped has six degrees of freedom in space, i.e., three degrees of freedom of movement and three degrees of freedom of rotation. To ensure that the part has a uniquely defined position and to completely eliminate the degrees of freedom of the part in the assembly system, a “3-2-1” positioning scheme is generally used, consisting of the following. (1) Three positioning blocks to constrain the part to move in the z-direction in the atypical structural dimension plane and to rotate in two directions in the typical structural dimension projection plane, the normal plane. (2) A four-way locating circular pin that fits into a circular hole in the part and constrains the movement of the part in the x and y directions in the typical structural dimension plane. (3) A two-way locating long hole pin that fits into a slotted hole in the part and limits the rotation of the part in one direction in the typical structural dimensional plane. Failure of the positioning and clamping elements can lead to deviations in the positioning of the part in the assembly system, which, in turn, affects the geometry and assembly accuracy of the product. For the “3-2-1” positioning method, the deviations of

the part in the typical and atypical structural dimensional planes are independent and can be analyzed separately.

### 2.2. Description of Typical Structural Dimensional Plane Deviations

The layout of the fixture for the part in the typical structural dimension plane  $xoy$  is shown in Figure 2a.  $P_i$  is the four-way locating round hole pin and  $P_{i+1}$  is the two-way locating long hole pin.

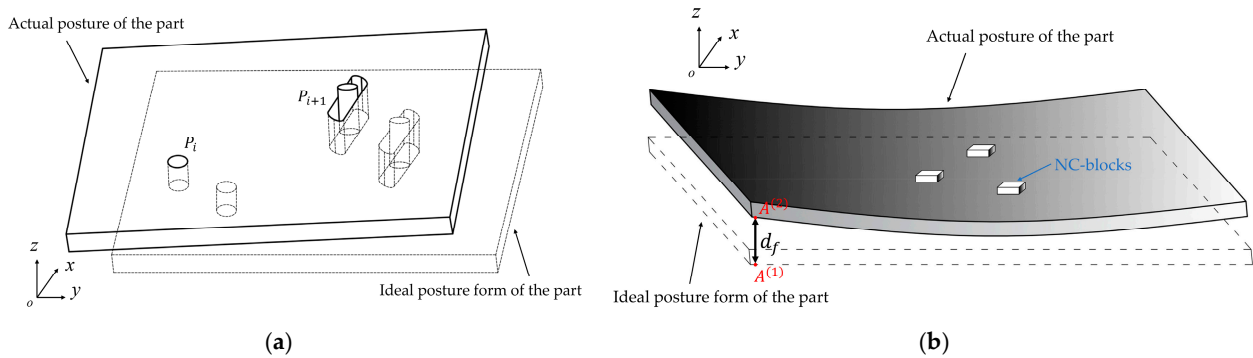


**Figure 2.** (a) Fixture layout diagram in plane  $xoy$ . (b) Fixture layout diagram in plane  $yoz$ .

### 2.3. Description of Atypical Structural Dimensional Plane Deviations

In the actual assembly system, for weakly rigid parts, the “3-2-1” positioning scheme is not sufficient to support the deformation of the part in the atypical part size direction, i.e., assume any point  $A$ , the flexible deformation  $d_f$  of point  $A$  in the  $z$  direction must be taken into account. The layout of the fixture for the part in the atypical structural dimension plane  $yoz$  is shown in Figure 2b.

### 2.4. Illustration of the Deviation State Space Model for a Multi-Level Assembly Process (MAP)

In the typical structural dimension plane, the structural rigidity of the part is sufficient and the part deviation is manifested as the overall translation or rotation, whereas in the atypical structural dimension plane, the structural rigidity of the part is extremely poor compared to the former and the part deviation is manifested as local warping or twisting deformation.

Therefore, the following assumptions are made for the deviation transfer model of a multi-level assembly of a three-dimensional weakly rigid part. (1) The deviations of the part in the typical and atypical structural dimension planes are independent of each other. (2) The part is positioned according to the “3-2-1” positioning principle, ignoring the wear of the NC blocks and the limiting effect of the blocks on the flexible deviation of the part. (3) The positioning elements of the fixture already involved in the assembly are not invalidated until the end of the overall assembly process.

## 3. Deviation Analysis of Weakly Rigid Parts

The deviation of a weakly rigid part is the amount of deviation in the current assembly station relative to the theoretical position of the part at the time of design.

### 3.1. Part Deviation

In terms of the spatial coordinate system, part deviations can be decomposed into rigid translations and rigid rotations along the  $x$ ,  $y$  and  $z$  directions and, for weakly rigid parts, flexible bending deformations in specific directions.

#### ① Typical structural dimensional planes:

For weakly rigid thin-walled parts of the wall plate type shown in Figure 1, there are deviations along the  $x$  and  $y$  directions and rotations in the  $\sigma$  plane.

#### ② Atypical structural dimensional planes:

To reduce the redundancy of the state space model, the wear of the locating block and the deviation of the part from rigid rotation in the  $\tau$  and  $\varphi$  planes are neglected. The deviations of the part in the atypical structural dimension plane are projected in the direction of its long axis, i.e., to the  $\varphi$  plane, as shown in Figure 1.

At station  $k$ , for a point  $A$  on the part, the part deviation vector is noted as:

$$\Delta X_A = [\Delta x_A(k), \Delta y_A(k), \Delta z_A(k), \Delta\alpha(k), \Delta\beta_A(k)]^T \tag{1}$$

In Equation (1),  $\{\Delta x_A(k), \Delta y_A(k), \Delta z_A(k)\}$  are the offsets of point  $A$  on the part along the  $x$ ,  $y$  and  $z$  directions,  $\{\Delta\alpha\}$  is the rigid rotation deviation of the typical structural dimension plane of the part on the part, and  $\{\Delta\beta_A\}$  is the flexible rotation deviation of point  $A$  on the part in the projection plane.

For any two points  $A$  and  $B$  on part 1, their deviations in the  $\sigma$  plane are shown in Figure 3.  $A$  and  $B$  are the theoretical positions of the two points,  $A'$  and  $B'$  are the actual positions of the two points and the equidistant parallel line  $A'B''$  of  $AB$  is made with point  $A'$  as the base point. According to the vector operation theorem, the relative deviation (line  $B'A'$ ) between point  $A'$  and point  $B'$  has:

$$\begin{aligned} \overrightarrow{B'A'} &= \overrightarrow{B'B} - \overrightarrow{A'A} \\ \overrightarrow{B''B} &= \overrightarrow{A'A} \\ \overrightarrow{B'A'} &= \overrightarrow{B'B} - \overrightarrow{B''B} = \overrightarrow{B'B''} \end{aligned} \tag{2}$$

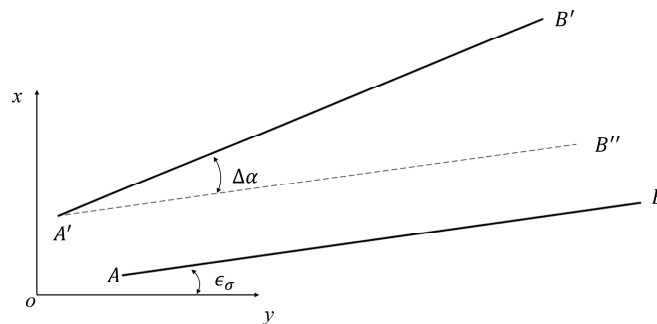


Figure 3. Diagram of the deviation of two points on a part in the  $\sigma$  plane.

At this time, the relative deviation between  $A'$  and  $B'$  ( $B'A'$ ) is transformed into the relative deviation between  $B'$  and  $B''$  ( $B'B''$ ).

Assuming that the deviations of point  $A$  and point  $B$  in the  $\sigma$  plane are  $\Delta x_A, \Delta y_A, \Delta\alpha$  and  $\Delta x_B, \Delta y_B, \Delta\alpha$ , respectively, then the deviations of point  $B$  from point  $A$  in the  $\sigma$  plane are related as:

$$\begin{aligned} \begin{bmatrix} \Delta x_B \\ \Delta y_B \end{bmatrix} &= \begin{bmatrix} \Delta x_A \\ \Delta y_A \end{bmatrix} + \begin{bmatrix} \|H_{B,A}^\sigma\|_2 \Delta\alpha \cos\epsilon_\sigma \\ -\|H_{B,A}^\sigma\|_2 \Delta\alpha \sin\epsilon_\sigma \end{bmatrix} \\ \begin{bmatrix} \Delta x_B \\ \Delta y_B \end{bmatrix} &= \begin{bmatrix} 1 & 0 & \|H_{B,A}^\sigma\|_2 \cos\epsilon_\sigma \\ 0 & 1 & -\|H_{B,A}^\sigma\|_2 \sin\epsilon_\sigma \end{bmatrix} \cdot \begin{bmatrix} \Delta x_A \\ \Delta y_A \\ \Delta\alpha \end{bmatrix} \end{aligned} \tag{3}$$

In Equation (3),  $H_{B,A}^\sigma = [y_A - y_B, x_A - x_B]^T$  represents the distance vector between the coordinates of two points  $B_1$  and  $A_1$  on the  $\sigma$  plane,  $\|H_{B,A}^\sigma\|_2$  is the 2-parametric number of this vector and  $\epsilon_\sigma$  is the angle between the line connecting two points  $B_1$  and  $A_1$  on the  $\sigma$  plane and the  $y$  axis.

For any two points  $A$  and  $C$  on part 1, their deviation in the  $\varphi$  plane is shown in Figure 4. Since the rigid rotation deviation of the part in the  $\tau$  and  $\varphi$  planes is neglected, only the flexible deformation in the  $z$  direction exists, and, because of its own gravity, the

uneven distribution of support forces and other factors, it can be considered that the flexible deformation of the part in the  $\varphi$  plane can be regarded as a smooth arc distributed along the y axis.

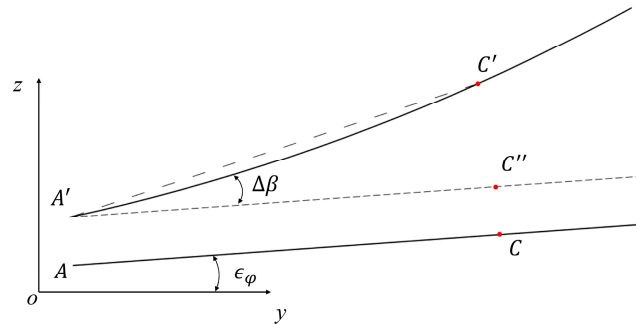


Figure 4. Diagram of the deviation of two points on a part in the  $\varphi$  plane.

Suppose the deviations of point A and point C in the  $\varphi$  plane are  $\Delta y_A, \Delta z_A, \Delta\beta$  and  $\Delta y_C, \Delta z_C, \Delta\beta$ , respectively, then the deviation of point C from point A in the  $\varphi$  plane is related to

$$\begin{aligned} [\Delta z_C] &= [\Delta z_A] + [\|H_{C,A}^\varphi\|_2 \Delta\beta \cos\epsilon_\varphi] \\ [\Delta z_C] &= [1 \quad \|H_{C,A}^\varphi\|_2 \cos\epsilon_\varphi] \cdot \begin{bmatrix} \Delta z_C \\ \Delta\beta \end{bmatrix} \end{aligned} \tag{4}$$

In Equation (4),  $\epsilon_\varphi$  is the angle between the line connecting the two points  $C_1$  and  $A_1$  on the  $\varphi$  plane and the x axis.

Assembling the two matrix Equations (3) and (4), the part deviation relationship represented by any two points A, B on part 1 is obtained as follows:

$$\Delta X_{B_1} = E_{B_1, A_1} \cdot \Delta X_{A_1} \tag{5}$$

$$E_{B,A} = \begin{bmatrix} 1 & 0 & 0 & \|H_{B,A}^\sigma\|_2 \cos\epsilon_\sigma & 0 \\ 0 & 1 & 0 & -\|H_{B,A}^\sigma\|_2 \sin\epsilon_\sigma & 0 \\ 0 & 0 & 1 & 0 & \|H_{B,A}^\varphi\|_2 \cos\epsilon_\varphi \\ 0 & 0 & 0 & 1 & 0 \\ 0 & 0 & 0 & 0 & 1 \end{bmatrix} \tag{6}$$

### 3.2. Sources of Deviation

From the point of view of the sources of deviation, the part deviation is a state vector in the state space model. The part deviation consists of three sources of deviation as follows:

- The part has an initial manufacturing deviation  $\Delta M$ , which is determined by the processing and manufacturing technology level and the transportation and preservation conditions of the part. Because the assembly station  $k > 0$ , so  $\Delta X(0) = \Delta M$ .
- The part has a deviation due to the deviation of the clamping element  $U(k)$ .
- The part has a deviation caused by the contact force  $T(k)$  in the assembly fitting area.

### 4. Deviations in the Fixture Positioning and the Resulting Part Deviations

After clamping, since the “3-2-1” positioning scheme has a very limited effect of the positioning block on the flexible deviation of the part, the influence of the positioning block on the flexible deviation of the part is ignored, the wear of the positioning block is not taken into account and the flexible deviation of the part due to insufficient rigidity is regarded as the positioning deviation. Then, the deviation of the fixture includes the four-way positioning round hole pin and the fixture deviation includes the movement deviation in the  $\sigma$  plane of the two-way positioning long hole pins and the flexible deformation in the  $\varphi$

plane of the two positioning pins. At station  $k$ , the set of deviations of the two locating pins  $P_1$  and  $P_2$  along the  $x, y, z$  directions is noted as  $\{\Delta U_{P_1}(k), \Delta U_{P_2}(k)\}$  as:

$$\{\Delta U_{P_1}(k), \Delta U_{P_2}(k)\} = \{\Delta x_{P_1}(k), \Delta y_{P_1}(k), \Delta z_{P_1}(k), \Delta x_{P_2}(k), \Delta y_{P_2}(k), \Delta z_{P_2}(k)\} \quad (7)$$

4.1. Fixture Deviation

① Typical structural dimension planes:

Part positioning adopts the “3-2-1” positioning method.  $P_1$  and  $P_2$  are the theoretical positions of two points;  $P_1'$  and  $P_2'$  are the actual positions of two points. For the two positioning points  $P_1$  and  $P_2$  on the  $\sigma$  plane of part 1, the deviations are shown in Figure 5.

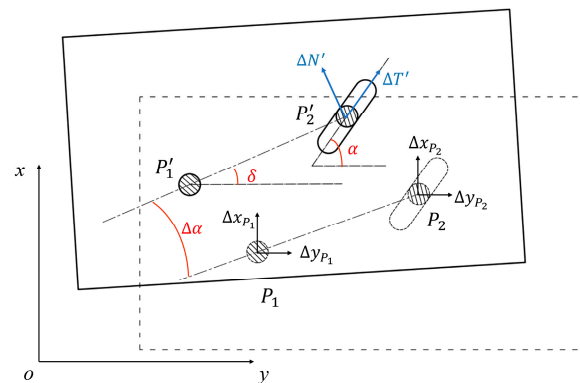


Figure 5. Diagram of the deviation of two positioning points  $P_1$  and  $P_2$  on the  $\sigma$  plane.

Assume that the angle between the two positioning points  $P_1'$  and  $P_2'$  and the  $y$  axis is  $\delta$ , and the angle between the long-axis direction of the slot of the two-way positioning pin  $P_2'$  and the  $y$  axis is  $\alpha$ . The relative deviation of  $P_1'$  and  $P_2'$  is decomposed into a deviation  $\Delta T'$  along the long axis of the slot of the two-way locating long hole pin and a deviation  $\Delta N'$  perpendicular to the line connected to  $P_1'$  and  $P_2'$ . Since the two-way locating long hole pin can be moved in the slot along the long-axis direction,  $\Delta T'$  does not affect the positioning accuracy of the fixture, i.e., it does not cause deviation of the part and can be ignored, but  $\Delta N'$  will cause the part to produce a rotation deviation on the fixture, and this deviation is rigid.

Assume the deviations of points  $P_1$  and  $P_2$  in the  $\sigma$  plane are  $\Delta x_{P_1}, \Delta y_{P_1}$  and  $\Delta x_{P_2}, \Delta y_{P_2}$ , respectively. According to the sine theorem, decomposing the relative deviations  $\Delta x_{P_2}, \Delta y_{P_2}$  and  $\Delta y_{P_2} - \Delta y_{P_1}$  of the two locus points into the vertical direction of the line  $P_1'P_2'$ , we get:

$$\frac{\Delta N_1'}{\sin \delta_1} = \frac{\Delta x_{P_2} - \Delta x_{P_1}}{\sin \delta_2}, \frac{\Delta N_2'}{\sin \delta} = \frac{\Delta y_{P_2} - \Delta y_{P_1}}{\sin \delta_3} \quad (8)$$

$$\Delta N' = \langle c\alpha \rangle \cdot \Delta N_1' + \left\langle c\left(\alpha + \frac{\pi}{2}\right) \right\rangle \Delta N_2' \quad (9)$$

In Equations (8) and (9),  $c\left(\alpha + \frac{\pi}{2}\right) = \cos\left(\alpha + \frac{\pi}{2}\right)$ ,  $\delta_1 = \frac{\pi}{2} - \alpha$ ,  $\delta_2 = \frac{\pi}{2} + \alpha - \delta$ ,  $\delta_3 = \frac{\pi}{2} + \delta - \alpha$ , the operator  $\langle c\alpha \rangle$  denotes  $\frac{c\alpha}{|c\alpha|} = \pm 1$ . This gives the part rotation deviation  $\Delta\alpha$  due to the two locating pins as:

$$\Delta\alpha = \frac{\Delta N'}{\|H_{P_1, P_2}^\sigma\|_2} \quad (10)$$

② Atypical structural dimension planes:

Assume the deviations of two positioning points  $P_1$  and  $P_2$  in the  $\varphi$  plane are as shown in Figure 6 and assume the angle between the straight lines connected to the  $y$  axis at the actual positions of the two positioning points  $P_1'$  and  $P_2'$  are  $\theta$ . Decompose the relative

deviation of  $P_1'$  and  $P_2'$  into the deviation  $\Delta T''$  along the linear direction of line  $P_1P_2$  and the deviation  $\Delta N''$  in the vertical direction of line  $P_1P_2$ .

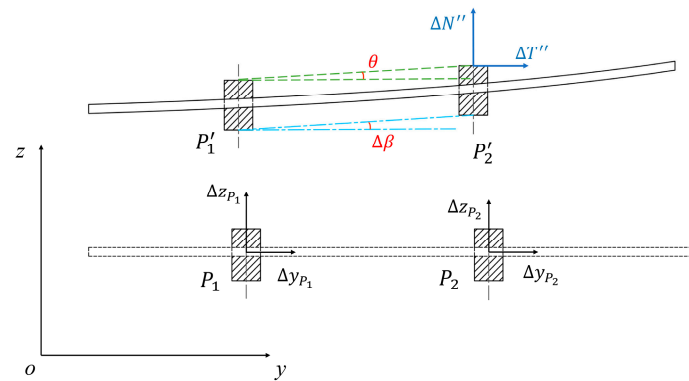


Figure 6. Diagram of the deviation of two positioning points  $P_1$  and  $P_2$  on the  $\varphi$  plane.

Suppose the deviations of points  $P_1$  and  $P_2$  in the  $\varphi$  plane are  $\Delta y_{P_1}, \Delta z_{P_1}$  and  $\Delta y_{P_2}, \Delta z_{P_2}$ , respectively, and the relative deviations of the two locus points  $P_1$  and  $P_2$  are  $\Delta y_{P_2} - \Delta y_{P_1}$  and  $\Delta z_{P_2} - \Delta z_{P_1}$ . Decomposing the relative deviation into the vertical direction of the line  $P_1P_2$  gives:

$$\frac{\Delta T_1''}{\cos\theta} = \Delta z_{P_2} - \Delta z_{P_1}, \quad \frac{\Delta T_2''}{\sin\theta} = \Delta y_{P_2} - \Delta y_{P_1} \tag{11}$$

$$\Delta T'' = \langle c\theta \rangle \cdot \Delta T_1'' + \left\langle c\left(\theta + \frac{\pi}{2}\right) \right\rangle \cdot \Delta T_2'' \tag{12}$$

Since the parts studied in this paper are thin-walled parts and the positioning holes are all through-holes, it can be assumed that  $P_1P_2$  coincides with the  $y$  axis, i.e.,  $\theta = 0$ . Therefore,  $\Delta T''$  has nothing to do with the flexible deformation of the part, and  $\Delta N''$  makes the flexible deformation at point  $P_2$  relative to point  $P_1$ . Then the flexible bending deformation angle  $\Delta\beta'$  at point  $P_2$  with respect to point  $P_1$  is:

$$\Delta\beta' = \frac{\Delta T''}{\|H_{P_1, P_2}^\varphi\|_2} \tag{13}$$

The above equations are assembled to obtain the relationship between the deviation vector  $\Delta X_{P_1}$  of the positioning point  $P_1$  on the part and the set of deviation vectors  $\{\Delta U_{P_1}(k), \Delta U_{P_2}(k)\}$  of the fixture elements:

$$\Delta X_{P_1}(k) = G_{P_1, P_2} \cdot \begin{bmatrix} \Delta U_{P_1}(k) \\ \Delta U_{P_2}(k) \end{bmatrix} \tag{14}$$

$$G_{P_1, P_2} = \begin{bmatrix} 1 & 0 & 0 & 0 & 0 & 0 \\ 0 & 1 & 0 & 0 & 0 & 0 \\ 0 & 0 & 1 & 0 & 0 & 0 \\ \frac{-\langle c\alpha_{new} \rangle \cos\alpha}{\|H_{P_1, P_2}^\sigma\|_2 \cos\gamma} & \frac{-\langle c(\delta + \frac{\pi}{2}) \rangle \sin\alpha}{\|H_{P_1, P_2}^\sigma\|_2 \cos\gamma} & 0 & \frac{\langle c\alpha_{new} \rangle \cos\alpha}{\|H_{P_1, P_2}^\sigma\|_2 \cos\gamma} & \frac{\langle c(\delta + \frac{\pi}{2}) \rangle \sin\alpha}{\|H_{P_1, P_2}^\sigma\|_2 \cos\gamma} & 0 \\ 0 & \frac{-\langle c(\theta + \frac{\pi}{2}) \rangle \sin\theta}{\|H_{P_1, P_2}^\varphi\|_2} & \frac{-\langle c\theta \rangle \cos\theta}{\|H_{P_1, P_2}^\varphi\|_2} & 0 & \frac{\langle c(\theta + \frac{\pi}{2}) \rangle \sin\theta}{\|H_{P_1, P_2}^\varphi\|_2} & \frac{\langle c\theta \rangle \cos\theta}{\|H_{P_1, P_2}^\varphi\|_2} \end{bmatrix} \tag{15}$$

In Equation (15),  $\gamma = \alpha - \delta$ . In order to make the coefficient matrix  $G_{P_1, P_2}$  universal, a correction to  $\alpha$  is required:  $\alpha_{new} = \langle s\delta \rangle \cdot \alpha, s\delta = \sin\delta$ .

#### 4.2. Part Deviations Due to Fixture Deviations

① Typical structural dimensional planes:

At station  $k$ , it follows from Equation (3) that the deviation of any point  $A$  on part 1 from the positioning point  $P_1$  is as follows:

$$\begin{bmatrix} \Delta x_A \\ \Delta y_A \end{bmatrix} = \begin{bmatrix} 1 & 0 \\ 0 & 1 \end{bmatrix} \begin{bmatrix} \|H_{A,P_1}^\sigma\|_2 \cos \epsilon_\sigma \\ -\|H_{A,P_1}^\sigma\|_2 \sin \epsilon_\sigma \end{bmatrix} \cdot \begin{bmatrix} \Delta x_{P_1} \\ \Delta y_{P_1} \\ \Delta \alpha \end{bmatrix} \quad (16)$$

② Atypical structural dimensional planes:

As can be seen from the previous section, the flexible deformation of the part in the  $\varphi$  plane can be regarded as an arc, and the flexible bending deformation angle  $\Delta\beta$  varies at different coordinate points. As shown in Figure 7, any point  $A$  on the part,  $A'$  is the actual position of the point, and  $P_1'$  and  $P_2'$  are taken as the base points to make equal parallel lines  $P_1'P_2''$  and  $P_2'P_2'''$  of line  $P_1P_2$ , respectively, and  $\angle P_2'P_1'P_2''$  is noted as  $\Delta\beta'$ ,  $\angle A'P_1'P_2'''$  is  $\Delta\beta$ . When the point  $A'$  is located at position  $A_a'$  in Figure 7a, the relationship between the corresponding  $\Delta\beta$  and  $\Delta\beta'$  is as follows:

$$\Delta\beta = \Delta\beta' - \frac{180 \cdot \|H_{A,P_2}^\varphi\|_2}{2\pi \cdot \rho_{A,P_1,P_2}}, \Delta\beta' > 0 \quad (17)$$

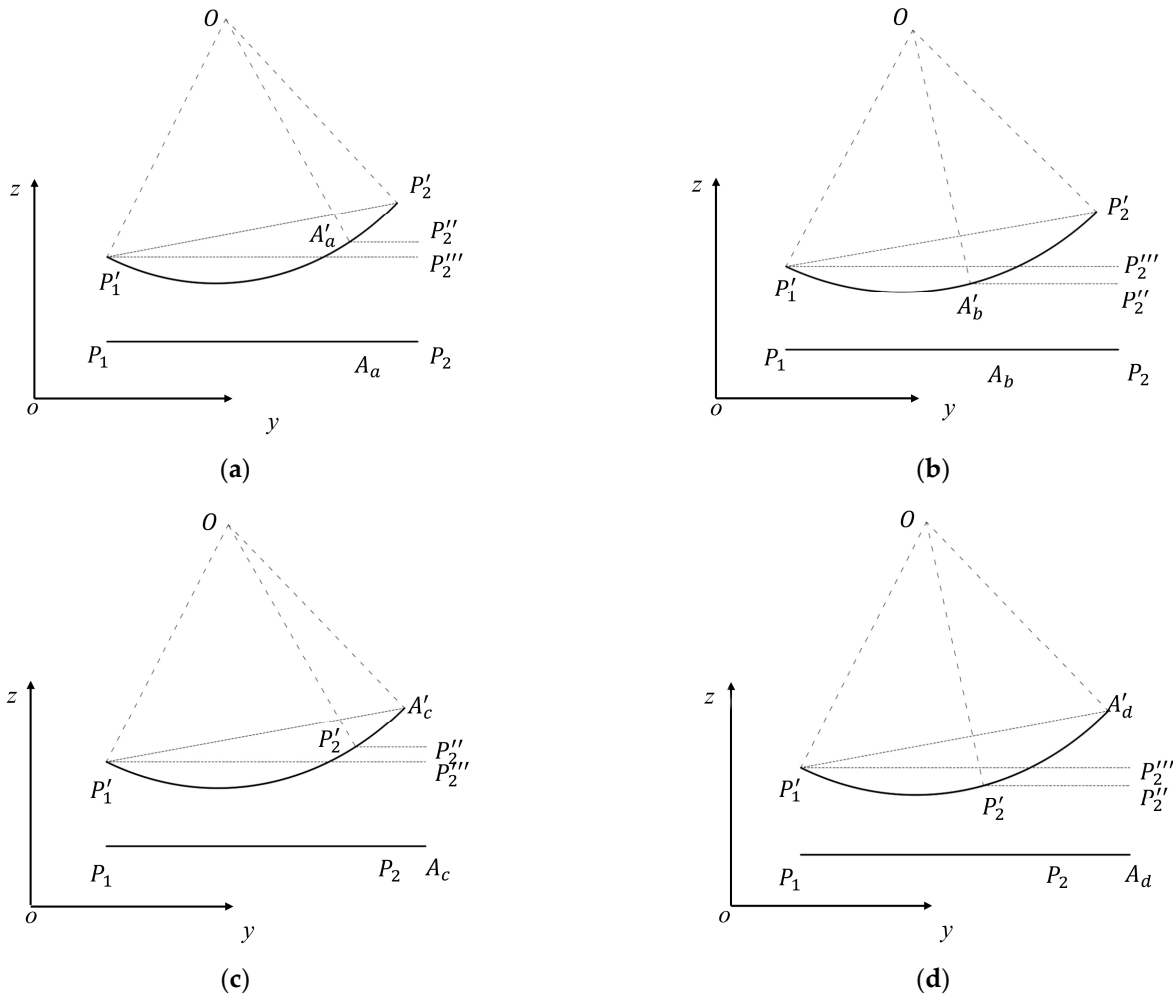


**Figure 7.** (a) point  $A'$  is located at position  $A_a'$ . (b) point  $A'$  is located at position  $A_b'$ . (c) point  $A'$  is located at position  $A_c'$ . (d) point  $A'$  is located at position  $A_d'$ .

When the point  $A'$  is located at position  $A_b'$  in Figure 7a, the relationship between the corresponding  $\Delta\beta$  and  $\Delta\beta'$  is as follows:

$$\Delta\beta = \Delta\beta' - \frac{180 \cdot \|H_{A,P_2}^\varphi\|_2}{2\pi \cdot \rho_{A,P_1,P_2}}, \Delta\beta' > 0 \tag{18}$$

When the point  $A'$  is located at position  $A_c'$  in Figure 7c, the relationship between the corresponding  $\Delta\beta$  and  $\Delta\beta'$  is as follows:

$$\Delta\beta = \Delta\beta' + \frac{180 \cdot \|H_{A,P_2}^\varphi\|_2}{2\pi \cdot \rho_{A,P_1,P_2}}, \Delta\beta' > 0 \tag{19}$$

When the point  $A'$  is located at position  $A_d'$  in Figure 7d, the relationship between the corresponding  $\Delta\beta$  and  $\Delta\beta'$  is as follows:

$$\Delta\beta = \Delta\beta' + \frac{180 \cdot \|H_{A,P_2}^\varphi\|_2}{2\pi \cdot \rho_{A,P_1,P_2}}, \Delta\beta' > 0 \tag{20}$$

From Equation (4), the deviation of any point  $A$  on the part from the positioning point  $P_1$  at station  $k$  is related as follows:

$$[\Delta z_A] = [1 \quad \|H_{A,P_1}^\varphi\|_2 \sin \epsilon_\varphi] \cdot \begin{bmatrix} \Delta z_{P_1} \\ \Delta\beta \end{bmatrix} \tag{21}$$

In summary, the deviation of any point  $A$  on the part is related to the deviation of the positioning point  $P_1$  as follows:

$$\Delta X_A = E_{A,P_1} \cdot F_{A,P_1} \cdot \Delta X_{P_1} \tag{22}$$

$$E_{A,P_1} = \begin{bmatrix} 1 & 0 & 0 & \|H_{A,P_1}^\sigma\|_2 \cos \epsilon_\sigma & 0 \\ 0 & 1 & 0 & -\|H_{A,P_1}^\sigma\|_2 \sin \epsilon_\sigma & 0 \\ 0 & 0 & 1 & 0 & \|H_{A,P_1}^\varphi\|_2 \cos \epsilon_\varphi \\ 0 & 0 & 0 & 1 & 0 \\ 0 & 0 & 0 & 0 & 1 \end{bmatrix} \tag{23}$$

$$F_{A,P_1} = \begin{bmatrix} 1 & 0 & 0 & 0 & 0 \\ 0 & 1 & 0 & 0 & 0 \\ 0 & 0 & 1 & 0 & 0 \\ 0 & 0 & 0 & 1 & 0 \\ 0 & 0 & 0 & 0 & 1 \pm \sin\left(\frac{180 \cdot \|H_{A,P_2}^\varphi\|_2}{2\pi \cdot \rho_{A,P_1,P_2}}\right) \cdot \frac{1}{\Delta\beta'} \end{bmatrix} \tag{24}$$

### 5. Assembly Contact Forces and Resulting Part Deviations

Due to the coupling of multiple sources of deviation, such as component manufacturing deviations and fixture deviations, there are deviations in the relative positions of the interconnected parts at the assembly point before the riveting or welding operation begins, particularly interference or gaps in the contact fit area of the assembly. In order to complete the assembly process, assembly forces are applied to the connected parts so that the deviations are closed in the contact fit area.

#### 5.1. Inspection of the Plane Position of the Assembly Contact Fit Area

Two parts to be assembled may have interference or gaps in the assembly contact fit area. If interference exists, the assembly force is applied to the two parts at the location of the interference or gap by the assembly plate before the riveting or welding operation to eliminate the impending interference or gap and to ensure that the assembly stresses

generated by the two parts in the assembly contact fit area are minimized. At this point in the assembly process, the part deformation caused by the assembly stresses between the two parts can be ignored and only the part deviation caused by the assembly forces on the assembly plate can be ignored.

Through flush coordinate transformation, the deviation vector of each part and the normal vector of the mating plane in the contact fit zone are unified in the global coordinate system, and the deviation of the measuring point of the part in the contact fit zone can be tested for contact relationship. To design a contact relationship detection algorithm for the contact fit planes, based on the vertex coordinates of the two fit planes, the normal vector of the two planes in the global coordinate system is used as the contact normal to detect whether there is interference or a gap between the two planes, and, thus, determine the fit of the two planes.

The Devillers and Guigue algorithm (Devillers’ algorithm) is a spatial triangle intersection detection algorithm that determines whether two triangles in space intersect in terms of the positivity or negativity of the determinant of each vertex on the triangle. The specific usage is as follows, the spatial position coordinates of four points in the known space:

$$A = [x_A \ y_A \ z_A]^T, B = [x_B \ y_B \ z_B]^T, C = [x_C \ y_C \ z_C]^T, D = [x_D \ y_D \ z_D]^T \quad (25)$$

define Equation (26) as the determinant algorithm 1:

$$|A \ B \ C \ D|_1 = \begin{vmatrix} x_A & y_A & z_A & 1 \\ x_B & y_B & z_B & 1 \\ x_C & y_C & z_C & 1 \\ x_D & y_D & z_D & 1 \end{vmatrix} = (A - D) \cdot (B - D) \times (C - D) \quad (26)$$

As shown in Figure 8, the four vertices of the contact fit area of part 1 and part 2 are connected to form quadrilaterals  $Q_1$  and  $Q_2$ . The vertices of  $Q_1$  and  $Q_2$  are noted as  $A_{Q_1}, B_{Q_1}, C_{Q_1}, D_{Q_1}$  and  $A_{Q_2}, B_{Q_2}, C_{Q_2}, D_{Q_2}$ , respectively, and the points  $A_{Q_1}, B_{Q_1}, C_{Q_1}$  and the points  $A_{Q_2}, B_{Q_2}, C_{Q_2}$  form triangles  $S_1$  and  $S_2$ . If the two triangles satisfy the intersection of space triangles test equation:

$$|A_{Q_1} \ B_{Q_1} \ A_{Q_2} \ B_{Q_2}|_1 \leq 0 \cap |A_{Q_1} \ C_{Q_1} \ A_{Q_2} \ C_{Q_2}|_1 \leq 0 \quad (27)$$

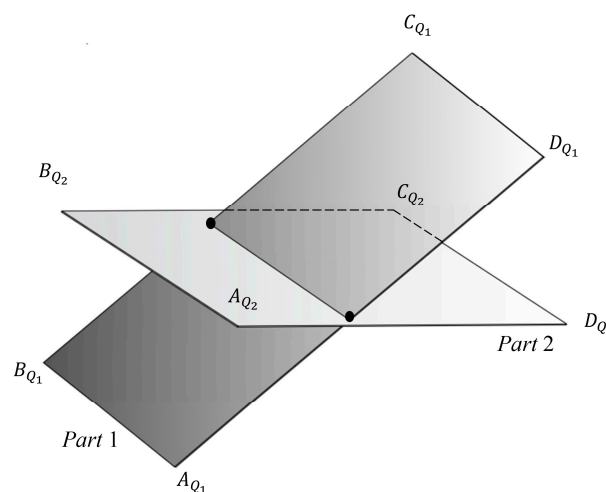


**Figure 8.** Interference and clearance between contact fit zone planes  $Q_1$  and  $Q_2$ . then the two triangles  $S_1$  and  $S_2$  intersect in space, i.e., the contact fit zone planes  $Q_1$  and  $Q_2$  are in both interference and clearance.

However, Devillers’ algorithm can only be used to determine whether two planes intersect, as shown in Figure 9, when the plane  $Q_1$  completely penetrates  $Q_2$ ; the penetration

relationship between the two planes cannot be correctly judged. Therefore, a spatial triangle penetration detection algorithm based on the deviation of the part measurement points is proposed to determine the penetration relationship between two triangles in space with the help of the positive and negative of the determinant formed by the deviation of each vertex on the plane triangle. Suppose the z direction be the contact normal direction and the points  $A_{Q_1}, B_{Q_1}, C_{Q_1}, A_{Q_2}, B_{Q_2}, C_{Q_2}$  in the contact normal direction deviation vector

$$\Theta_1 = [\Delta z_{A_{Q_1}} \quad \Delta z_{B_{Q_1}} \quad \Delta z_{C_{Q_1}}]^T, \quad \Theta_2 = [\Delta z_{A_{Q_2}} \quad \Delta z_{B_{Q_2}} \quad \Delta z_{C_{Q_2}}]^T \quad (28)$$

define Equation (29) as the determinant algorithm 2:

$$|\Theta_1 \quad \Theta_2|_2 = \begin{vmatrix} \Delta z_A & \Delta z_B & \Delta z_C \\ \Delta z_D & \Delta z_E & \Delta z_F \\ 1 & 1 & 1 \end{vmatrix}_2 = (\Delta z_A - \Delta z_D) \cdot (\Delta z_B - \Delta z_E) \cdot (\Delta z_C - \Delta z_F) \quad (29)$$

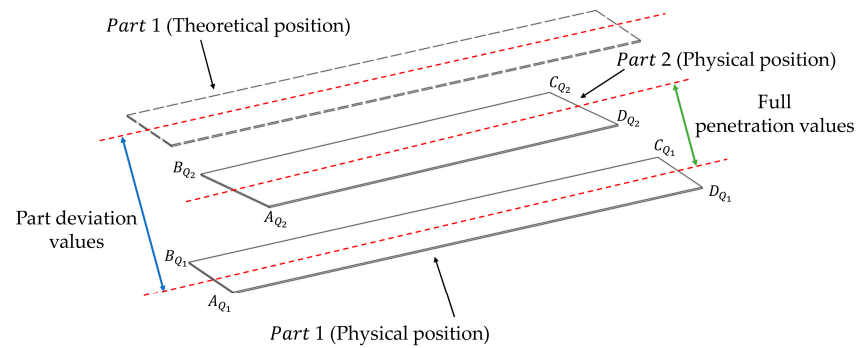


Figure 9. Part 1 is fully penetrated in part 2.

When the two planes  $Q_1$  and  $Q_2$  are judged not to intersect by the intersection detection algorithm, penetration detection is required for  $Q_1$  and  $Q_2$ . For the two triangles  $S_1$  and  $S_2$  within the planes  $Q_1$  and  $Q_2$ , the deviation vector  $\Theta_{S_1} = [\Delta z_{A_{S_1}} \quad \Delta z_{B_{S_1}} \quad \Delta z_{C_{S_1}}]^T$  and  $\Theta_{S_2} = [\Delta z_{A_{S_2}} \quad \Delta z_{B_{S_2}} \quad \Delta z_{C_{S_2}}]^T$  of their vertices  $A_{S_1}, B_{S_1}, C_{S_1}$  and  $A_{S_2}, B_{S_2}, C_{S_2}$ . Substitute the spatial triangle penetration detection equation  $|\Theta_1 \quad \Theta_2|_2$ . When  $|\Theta_1 \quad \Theta_2|_2 < 0$ ,  $S_1$  is completely penetrated by  $S_2$ , i.e., there is interference between the planes  $Q_1$  and  $Q_2$ . When  $|\Theta_1 \quad \Theta_2|_2 > 0$ , there is no penetration between  $S_1$  and  $S_2$ , i.e., there is a gap between the planes  $Q_1$  and  $Q_2$ . When  $|\Theta_1 \quad \Theta_2|_2 = 0$ ,  $S_1$  and  $S_2$  fit exactly together, i.e., there is neither interference nor a gap between the planes  $Q_1$  and  $Q_2$ .

### 5.2. Part Deviations Due to Assembly Contact Forces

In the theoretical case, assuming that there is a point  $A_1$  on part 1 for the riveted or welded connection position, there must exist a point  $A_2$  on part 2 which is connected to part 1. Points  $A_1$  and  $A_2$  coincide in space, and points  $A_1$  and  $A_2$  are recorded as a pair of assembly connection points in the assembly process, whether there is interference or a gap between the two assembly planes. According to the law of linear elasticity, assuming that a unit force  $F_A$  is applied to any point  $A$  on the part before riveting or welding, the displacement change at point  $A$  can be obtained as  $\delta_A = C_A \cdot F_A$ .  $C_A$  is the flexibility coefficient of point  $A$ , which indicates the displacement generated when point  $A$  is subjected to a unit force. From this, by dividing the part into a finite number of nodes, the relationship between the amount of displacement at all nodes and the force applied can be obtained:

$$[\delta] = [C] \cdot [F] \quad (30)$$

$$[F] = [K] \cdot [\delta] \quad (31)$$

In Equations (30) and (31),  $[\delta] = [\delta_A, \delta_B, \delta_C, \dots, \delta_N]^T$  denotes the amount of displacement of all nodes,  $[F] = [F_A, F_B, F_C, \dots, F_N]^T$  denotes the forces acting on all nodes;  $[C]$  is the multidimensional flexibility matrix of the part, representing the displacement produced by each node when all nodes on the part are subjected to a unit force;  $[K]$  is the multidimensional stiffness matrix of the part,  $[K] = [C]^{-1}$ .

Equations (30) and (31) can accurately explain the relationship between nodal forces and nodal displacements, where  $[\delta]$  and  $[F]$  contain information on the displacements and bearing forces of all nodes. At workstation  $k$ , part 1 and part 2, the two parts to be connected, are set to be assembled; in the global coordinate system, the flexibility matrix of the two are  $[C_1]$  and  $[C_2]$ , the two parts to be connected by the assembly forces are  $[F_1(k)]$  and  $[F_2(k)]$ , then the two parts' displacement  $[\delta_1(k)]$  and  $[\delta_2(k)]$  is:

$$[\delta(k)] = \begin{bmatrix} \delta_1(k) \\ \delta_2(k) \end{bmatrix} = [C(k)] \cdot \begin{bmatrix} F_1(k) \\ F_2(k) \end{bmatrix} = \begin{bmatrix} C_1 & \\ & C_2 \end{bmatrix} \cdot \begin{bmatrix} F_1(k) \\ F_2(k) \end{bmatrix} \tag{32}$$

In Equation (32),  $F_1(k) = [F_{A_1}(k) \ F_{B_1}(k) \ \dots \ F_{N_1}(k)]^T$ ,  $F_{A_1} = [f_{A_1x}(k) \ f_{A_1y}(k) \ f_{A_1z}(k)]^T$ ,  $\{A, B, \dots, N\}$  is the key point number on part 1,  $\{f_{A_1x}, f_{A_1y}, f_{A_1z}\}$  is the component of the assembly force at point  $A$  on part 1 on the  $xyz$  axis.  $\delta_1 = [\delta_{A_1}(k) \ \delta_{B_1}(k) \ \dots \ \delta_{N_1}(k)]^T$ ,  $\delta_{A_1} = [\Delta x_{A_1}(k) \ \Delta y_{A_1}(k) \ \Delta z_{A_1}(k)]^T$  indicates part deviation due to assembly forces at point  $A$  on part 1.

### 6. Deviation State Space Model for the MAP of Three-Dimensional Weakly Rigid Parts

In a multi-level assembly process, as the assembly process is extended, dimensional deviations of parts, fixture positioning deviations and assembly contact deviations accumulate gradually in the assembly body, forming dimensional deviations of the assembly at the end of the last assembly station, a process that can be mapped as a discrete event dynamic system for the transfer of assembly deviations of weakly rigid parts.

For a multi-station assembly system, the number of states corresponds to the number of assembly stations. Let a total of  $n$  assembly stations be included, i.e., there exist  $n$  state spaces, and the assembly operation at each station is mapped as a discrete event. Figure 10 shows a schematic diagram of the multi-level assembly of a three-dimensional part, and Figure 11 shows a schematic diagram of the state space of the multi-station assembly model for each part shown in Figure 10.

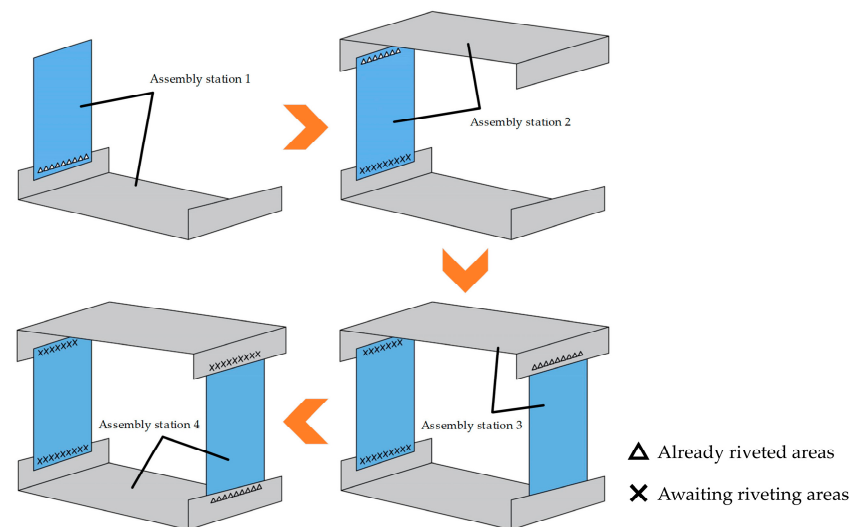


Figure 10. Four assembly stations for weakly rigid flat parts.

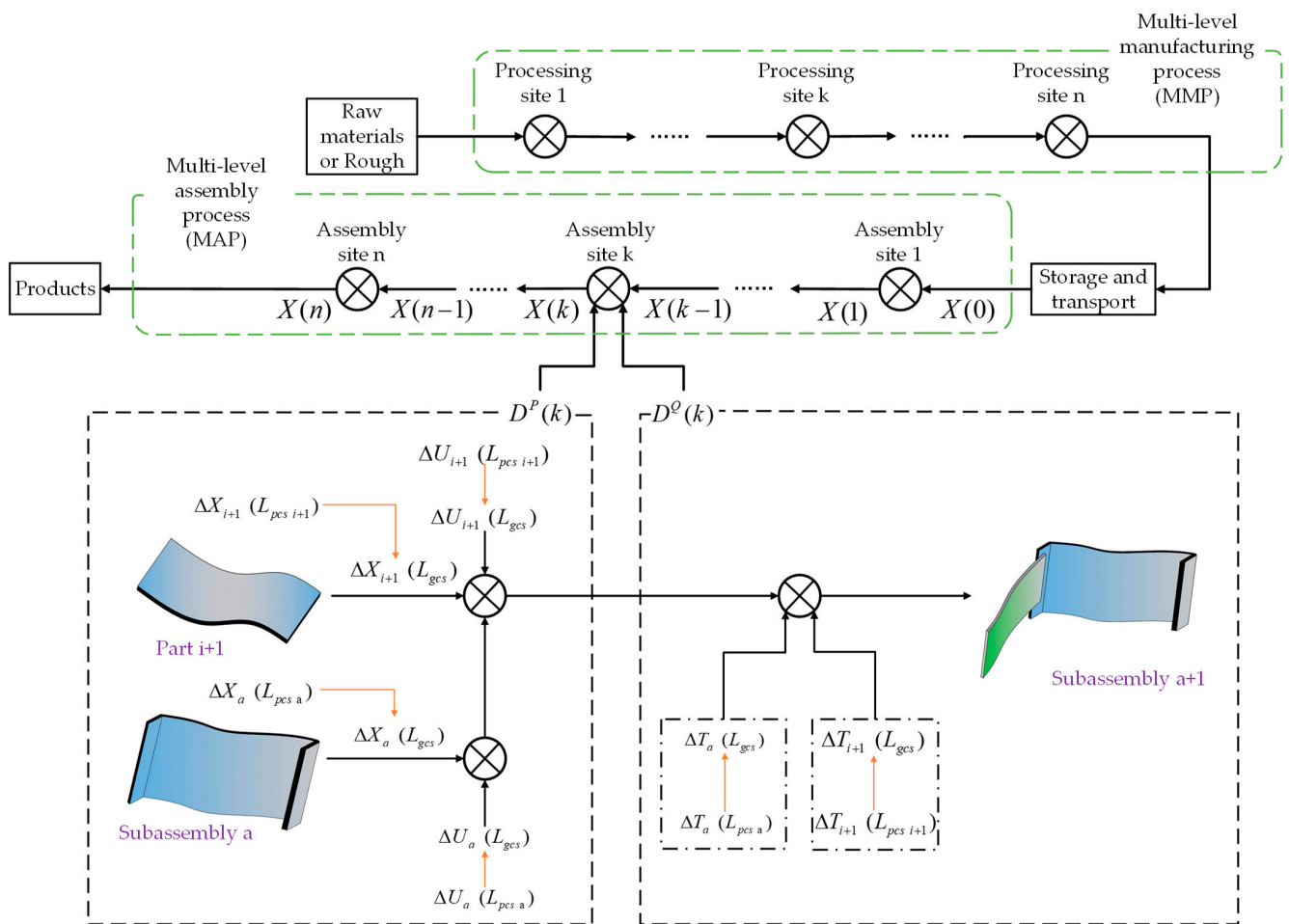


Figure 11. Diagram of the multi-working assembly state of a weakly rigid flat part.

At station  $k$ , independent part  $i+1$  completes clamping and riveting operations with sub-assembly part  $a$  at the previous assembly station to form sub-assembly part  $a+1$ . The sub-assembly part  $a+1$  then moves on to the next assembly station until the assembly process is completed to produce the total assembly.

### 6.1. Deviation Conversion from the Part to the Global Coordinate System

As mentioned earlier, from the perspective of modelling the deviation vectors of each part, each part has an independent part coordinate system  $L_{pcs}$ . For the angle joint assembly system, in the contact fit area of two parts, two contact surface normal vectors exist in each part coordinate system, and the un-unified two normal vectors greatly affect the modelling and calculation efficiency of the deviation flow state model. From the perspective of multi-station assembly flow modelling, a unified global coordinate system  $L_{gcs}$  is established and a mathematical relationship between the global coordinate system at the assembly level and the part coordinate system at the part level is established by means of a homogeneous transformation matrix.

Figure 12 has the local coordinate systems  $L_{pcs1}$  and  $L_{pcs2}$  of part 1 and part 2 and the global coordinate system  $L_{gcs}$  of the assembly system. According to the right-handed spiral criterion specifying the positive direction of rotation of the coordinate axes, the rotation vector angles of  $x$ ,  $y$  and  $z$  of coordinate system  $L_{pcs1}$  with respect to coordinate system  $L_{gcs}$  are noted as  $\omega_x, \omega_y, \omega_z$  and the origin of coordinate system  $L_{pcs1}$ . The translation vector displacement of the origin of the coordinate system  $L_{pcs1}$  with respect to the origin of the coordinate system  $L_{gcs}$  is noted as  $t_x, t_y, t_z$ .

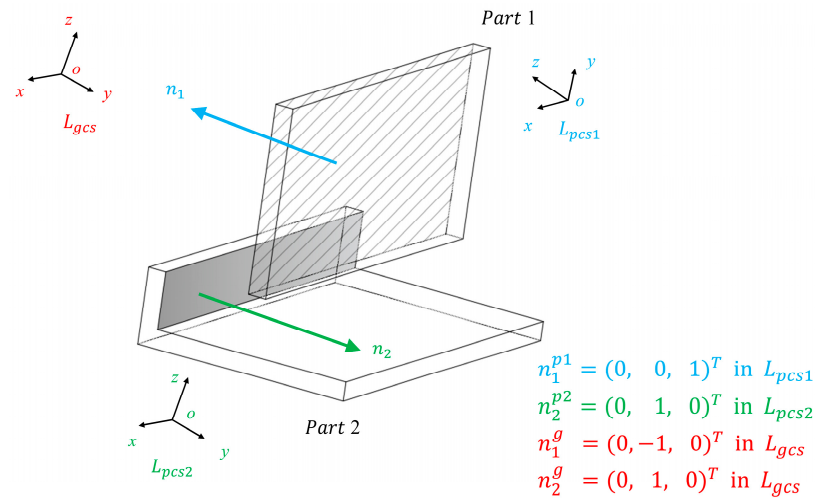


Figure 12. Normal vectors of contact surfaces on two parts.

With the introduction of the global coordinate system  $L_{gcs}$ , the normal vectors  $n_1^{p1}$  and  $n_2^{p2}$  of the non-uniform coordinate system in Figure 12 can be transformed into the normal vectors  $n_1^g$  and  $n_2^g$  of the uniform coordinate system, and the rotation transformation matrix from the coordinate system  $L_{pcs1}$  to the coordinate system  $L_{gcs}$  can be found as  $R_{p1/g}$  and translational transformation matrix  $T_{p1/g}$ :

$$R_{p1/g} = \begin{bmatrix} c\omega_z c\omega_y & c\omega_z s\omega_y s\omega_x - s\omega_z c\omega_x & c\omega_z s\omega_y c\omega_x + s\omega_z s\omega_x \\ s\omega_z c\omega_y & s\omega_z s\omega_y s\omega_x + c\omega_z c\omega_x & s\omega_z s\omega_y c\omega_x - c\omega_z s\omega_x \\ -s\omega_y & c\omega_y s\omega_x & c\omega_y c\omega_x \end{bmatrix}, T_{p1/g} = \begin{bmatrix} t_x \\ t_y \\ t_z \end{bmatrix} \quad (33)$$

At station  $k$ , note that  $X_{A_1}^{p1}(k) = [x_{A_1}^{p1}(k), y_{A_1}^{p1}(k), z_{A_1}^{p1}(k), v]^T$  denotes the coordinates of the homogeneous position coordinates of point  $A$  in the coordinate system  $L_{pcs1}$  for any point  $A$  on part 1.  $\Delta X_{A_1}^{p1}(k) = [\Delta x_{A_1}^{p1}(k), \Delta y_{A_1}^{p1}(k), \Delta z_{A_1}^{p1}(k), \Delta \alpha^{p1}(k), \Delta \beta^{p1}(k)]^T$  denotes the vector of part deviations of point  $A$  in the coordinate system  $L_{pcs1}$ . Where  $v$  is the coordinate projection coefficient, then the relationship between the coordinates  $X_{A_1}^g(k)$  and  $X_{A_1}^{p1}(k)$  and the deviation vector  $\Delta X_{A_1}^g(k)$  and  $\Delta X_{A_1}^{p1}(k)$  of the homogeneous position coordinates of point  $A$  in the coordinate system  $L_{gcs}$  is:

$$\begin{aligned} X_{A_1}^g(k) &= \Lambda_1 \cdot X_{A_1}^{p1}(k) \\ \Delta X_{A_1}^g(k) &= \Pi_1 \cdot \Delta X_{A_1}^{p1}(k) \end{aligned} \quad (34)$$

$$\begin{aligned} \begin{bmatrix} x_{A_1}^g(k) \\ y_{A_1}^g(k) \\ z_{A_1}^g(k) \\ v \end{bmatrix} &= \begin{bmatrix} R_{p1/g} & T_{p1/g} \\ & 1 \end{bmatrix} \cdot \begin{bmatrix} x_{A_1}^{p1}(k) \\ y_{A_1}^{p1}(k) \\ z_{A_1}^{p1}(k) \\ v \end{bmatrix} \\ \begin{bmatrix} \Delta x_{A_1}^g(k) \\ \Delta y_{A_1}^g(k) \\ \Delta z_{A_1}^g(k) \\ \Delta \alpha_1^g(k) \\ \Delta \beta_1^g(k) \end{bmatrix} &= \begin{bmatrix} R_{p1/g} & \\ & 1 \\ & & 1 \end{bmatrix} \cdot \begin{bmatrix} \Delta x_{A_1}^{p1}(k) \\ \Delta y_{A_1}^{p1}(k) \\ \Delta z_{A_1}^{p1}(k) \\ \Delta \alpha_1^{p1}(k) \\ \Delta \beta_1^{p1}(k) \end{bmatrix} \end{aligned} \quad (35)$$

In Equation (34), due to the absence of projection transformation,  $v$  constant to 1,  $\Lambda_1$  is the homogeneous transformation matrix of the position coordinates of the part from the coordinate system  $L_{pcs1}$  to the coordinate system  $L_{gcs}$ .  $\Pi_1$  is the transformation matrix of the part deviation vector from the coordinate system  $L_{pcs1}$  to the coordinate system  $L_{gcs}$ ; substituted into  $R_{p1/g}$  and  $T_{p1/g}$  the following can be obtained:

$$\begin{aligned}
 \begin{bmatrix} x_{A_1}^g(k) \\ y_{A_1}^g(k) \\ z_{A_1}^g(k) \\ 1 \end{bmatrix} &= \begin{bmatrix} c\omega_z c\omega_y & c\omega_z s\omega_y s\omega_x - s\omega_z c\omega_x & c\omega_z s\omega_y c\omega_x + s\omega_z s\omega_x & t_x \\ s\omega_z c\omega_y & s\omega_z s\omega_y s\omega_x + c\omega_z c\omega_x & s\omega_z s\omega_y c\omega_x - c\omega_z s\omega_x & t_y \\ -s\omega_y & c\omega_y s\omega_x & c\omega_y c\omega_x & t_z \\ & & & 1 \end{bmatrix} \begin{bmatrix} x_{A_1}^{p1}(k) \\ y_{A_1}^{p1}(k) \\ z_{A_1}^{p1}(k) \\ 1 \end{bmatrix} \\
 \begin{bmatrix} \Delta x_{A_1}^g(k) \\ \Delta y_{A_1}^g(k) \\ \Delta z_{A_1}^g(k) \\ \Delta \alpha_1^g(k) \\ \Delta \beta_1^g(k) \end{bmatrix} &= \begin{bmatrix} c\omega_z c\omega_y & c\omega_z s\omega_y s\omega_x - s\omega_z c\omega_x & c\omega_z s\omega_y c\omega_x + s\omega_z s\omega_x & & & \\ s\omega_z c\omega_y & s\omega_z s\omega_y s\omega_x + c\omega_z c\omega_x & s\omega_z s\omega_y c\omega_x - c\omega_z s\omega_x & & & \\ -s\omega_y & c\omega_y s\omega_x & c\omega_y c\omega_x & & & \\ & & & 1 & & \\ & & & & 1 & \end{bmatrix} \begin{bmatrix} \Delta x_{A_1}^{p1}(k) \\ \Delta y_{A_1}^{p1}(k) \\ \Delta z_{A_1}^{p1}(k) \\ \Delta \alpha_1^{p1}(k) \\ \Delta \beta_1^{p1}(k) \end{bmatrix} \tag{36}
 \end{aligned}$$

6.2. Deviation State Equation of Weakly Rigid Parts in a MAP

In order to reflect the dimensional deviations of the product, features that have a significant impact on the quality of the product are usually selected as objects for monitoring and control, such as the dimensions of the parts and sub-assemblies that affect the assembly accuracy and assembly force, which are usually referred to as key characteristics (KC). KC are divided into two types: key product characteristics (KPC) and key control characteristics (KCC). KPC refer to dimensional characteristics that affect the performance and appearance of assembled components, such as the coordinates of measurement points reflecting the coaxiality of mating holes in sub-assembly components, etc.; KCC refer to the relevant tooling, processes, etc. that have an impact on assembly accuracy, and can be taken as points that are not on the product, such as the key location control characteristics (KLCC) of fixtures acting on the product, interference or clearance support elements (key contact control characteristics (KCCC)) where assembly forces are applied to the product.

In Section 3.2, the three main sources of part dimensional deviations were described. By combining the above sources of deviations, the equation of state for the transfer of part deviation flow at station  $k$  is obtained as

$$\begin{aligned}
 X(k) &= X(k-1) + D^P(k) + D^Q(k) + R(k) \\
 X(k) &= [\Delta X_{A_1}(k) \quad \Delta X_{B_1}(k) \quad \cdots \quad \Delta X_{N_1}(k) \quad \cdots \quad \Delta X_{A_w}(k) \quad \cdots \quad \Delta X_{N_w}(k)]^T \tag{37}
 \end{aligned}$$

In Equation (37),  $k = \{1, 2, 3, \dots\}$  denotes the number of stations in the overall assembly process,  $X(k)$  is a state variable indicating the dimensional deviation of all parts within  $L_{gcs}$ ,  $\{1, 2, \dots, w\}$  denotes all part numbers in the overall assembly process and  $\{A_1, B_1, \dots, N_1, A_w, \dots, N_w\}$  denotes the KPC points on parts  $1 \sim w$  with numbered  $A_1 \sim N_w$ . When  $k = 0$ ,  $X(0)$  denotes the manufacturing deviation of the part.  $D^P(k)$  is the part deviation due to fixture deviation,  $D^Q(k)$  is the part deviation due to interference or clearance errors at the contact locations between the parts to be assembled and  $R(k)$  is the random noise error due to uncertainties in the assembly, all three of which lie within  $L_{gcs}$ . In  $D^Q(k)$ , the rigid rotation deviation  $\Delta \alpha(k)$  and the flexible rotation deviation  $\Delta \beta(k)$  are noted as zero, since only part displacement information exists.

In Equation (37),  $D^P(k)$  is the deviation of the part due to fixture deviation, and the deviation of the KCC point on the part in relation to the KPC point can be seen in Section 4.2:

$$\begin{aligned}
 D^P(k) &= B(k) \cdot U(k) \\
 U(k) &= [\Delta U_{P_1}(k) \quad \Delta U_{P_2}(k) \quad \Delta U_{P_3}(k) \quad \cdots \quad \Delta U_{P_n}(k)]^T \tag{38}
 \end{aligned}$$

$$B(k) = \begin{bmatrix} \Pi_1 E_{A_1, P_1} F_{A_1, P_1} G_{P_1, P_2} & 0^{5 \times 6} & 0^{5 \times 6} & \dots & 0^{5 \times 6} \\ 0^{5 \times 6} & \Pi_2 E_{A_2, P_3} F_{A_2, P_3} G_{P_3, P_4} & 0^{5 \times 6} & \dots & 0^{5 \times 6} \\ 0^{5 \times 6} & 0^{5 \times 6} & \Theta_3 & & 0^{5 \times 6} \\ \vdots & \vdots & \vdots & & \vdots \\ 0^{5 \times 6} & 0^{5 \times 6} & 0^{5 \times 6} & \dots & \Theta \\ & & & \ddots & \\ & & & & 0^{5s \times 6s} \end{bmatrix} \tag{39}$$

$$\Theta = \Pi_w \cdot E_{A_w, P_i} \cdot F_{A_w, P_i} \cdot G_{P_i, P_{i+1}}$$

In Equations (38) and (39),  $\{P_1, P_2, P_3, \dots, P_n\}$  denotes all KCC point numbers in the entire assembly process,  $\{\Delta U_{P_i}(k), \Delta U_{P_{i+1}}(k)\} \subseteq \{\Delta U_{P_1}(k), \Delta U_{P_2}(k), \Delta U_{P_3}(k), \dots, \Delta U_{P_n}(k)\}$  and  $\{P_i, P_{i+1}\} \subseteq \{P_1, P_2, P_3, \dots, P_n\}$ .  $A_w$  represents KPC point A on part w,  $B(k)$  represents the combined influence matrix from KCC point deviation to KPC point deviation and  $\Pi_w$  represents the deviation vector transformation matrix of part w from coordinate system  $L_{pcs1}$  to coordinate system  $L_{gcs}$ .

In Equation (38),  $D^Q(k)$  is the deviation of the part due to the assembly force at the contact position between the parts to be assembled, and the deviation of the point KCCC from the point KPC on the part can be seen in Section 5.2:

$$D^Q(k) = S(k) \cdot C(k) \cdot T(k) \tag{40}$$

$$T(k) = [\Delta F_{A_1}(k) \quad \Delta F_{B_1}(k) \quad \dots \quad \Delta F_{N_w}(k)]^T$$

$$C(k) = \begin{bmatrix} C_1 & & & \\ & C_2 & & \\ & & \ddots & \\ & & & C_w \end{bmatrix} \tag{41}$$

In Equations (40) and (41), the Devillers spatial triangle intersection detection algorithm and the spatial triangle penetration detection algorithm based on the deviation of the part measurement points are used to obtain the assembly forces  $\{\Delta T_{A_1}(k), \Delta T_{B_1}(k), \dots, \Delta T_{N_w}(k)\}$  on all nodes on parts 1~w within  $L_{gcs}$ , and  $\{\Delta \delta_{A_1}(k), \dots, \Delta \delta_{Q_w}(k)\}$  denotes the displacements of all nodes on parts 1 to w within  $L_{gcs}$  due to assembly forces. As  $T(k)$  contains information on the bearing forces of all nodes of the part, the deviation vector of KPC points is selected using the selection square  $S(k)$ , which is a Boolean diagonal square containing only 0 or 1 elements, where the positions of the non-zero rows correspond to the KPC points;  $C(k)$  is the flexibility matrix of the part, feeding back the relationship between the bearing forces of the part nodes and the amount of node displacements.

For ease of application and arithmetic, the coefficient matrix  $B(k)$  in Equation (40) can be written as a linear combination of the sub coefficient matrices  $L(k)$ ,  $E(k)$ ,  $F(k)$  and  $G(k)$  as follows:

$$B(k) = L(k) \cdot E(k) \cdot F(k) \cdot G(k)$$

$$L(k) = \begin{bmatrix} \Pi_1 & & & \\ & \Pi_2 & & \\ & & \ddots & \\ & & & \Pi_w \end{bmatrix} \tag{42}$$

### 7. Case Validation and Analysis

In this paper, a state space-based assembly deviation transfer model is applied to the frame structure of the rear fuselage engine compartment of a certain type of aircraft as an experimental case. From the perspective of mathematical theory, the multi-level assembly deviation transfer model of the rear fuselage frame structure is constructed. Firstly, the positional information of each part before the assembly process starts is obtained, and the

spatial coordinates of the KPC and KCC points on the part are updated through a spatial triangle penetration detection algorithm based on the deviation of the part measurement points. Finally, the similarities and differences between the multi-level assembly deviation transfer mathematical model and the finite element simulation model are compared horizontally to analyse the accuracy and feasibility of the multi-level assembly deviation transfer model proposed in this paper.

### 7.1. Case Description

The rear fuselage engine compartment frame structure is a typical large-sized structural part, which is integrated by several holes, slots, ribs or long trusses, and serves as the skeleton of the rear fuselage part of the aircraft and affects the assembly accuracy of the rest of the components and the overall assembly of the aircraft skin. As the thickness of the parts in the frame structure is much less than the typical part size, it can be assumed that the assembly process for this frame structure is consistent with the assembly of weakly rigid parts. Figure 13 shows a simplified model schematic of the frame structure of the middle and rear fuselage of a type of aircraft. Figure 14 shows the distribution of the upper KPC points and KCC points of part 1~4. The structure consists of two large-size thin-walled structural parts (Part1, Part3) and two connecting parts (Part2, Part4). Part1 and Part3 are weakly rigid parts with significant flexible deformation characteristics. Part2 and Part4 have a double-layered structure and their flexible deformation is negligible.

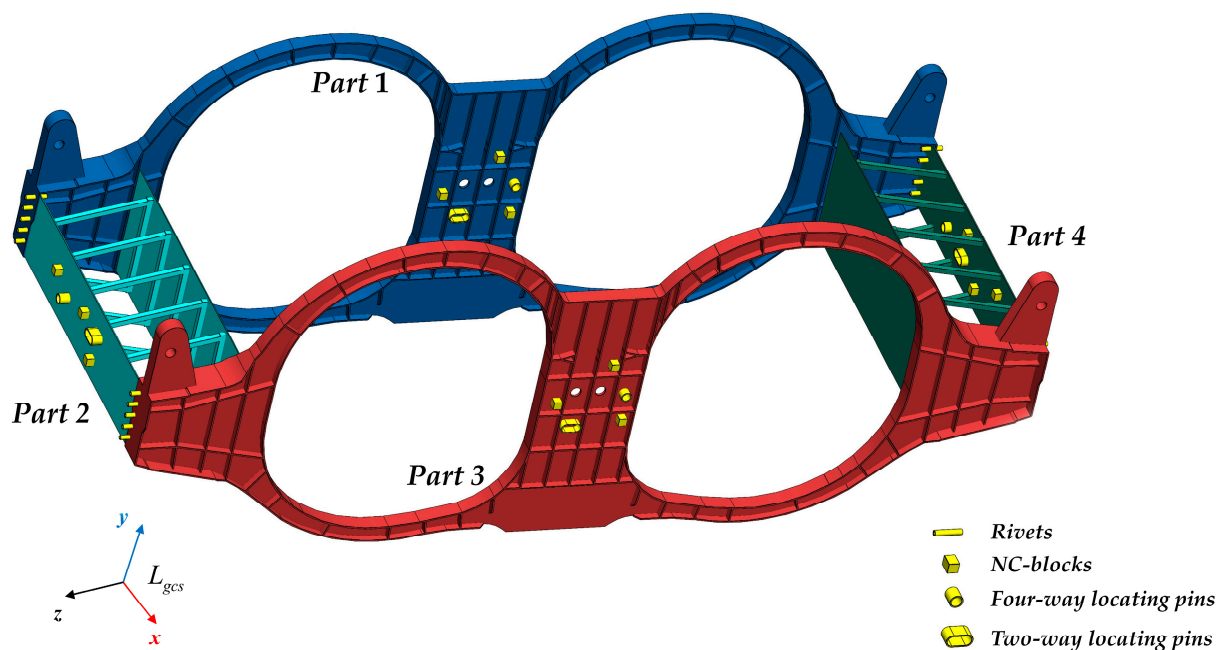


**Figure 13.** Diagram of the rear fuselage frame structure of the aircraft.

The assembly connection between the individual parts is completed by means of rivets. There are four stations on the assembly line, as shown in Figure 15. Station (I) is a preparatory station before the assembly process begins, the purpose of which is to measure the coordinates of the position of the KC points on each part and to position the thin-walled parts (Part1). Station (II) positions the connecting parts (Part2) and joins the thin-walled parts (Part1) to the connecting parts (Part2) to form the sub-assemblies (Part1 and 2). Workstation (III) positions the thin-walled parts (Part3), joining the subassemblies (Part1 and 2) to the thin-walled parts (Part3) to form subassemblies (Part1 and 2 and 3). Workstation (IV) positions the joiners (Part4) and joins the sub-assemblies (Part1 and 2 and 3) to the joiners (Part4) to form the sub-assemblies (Part1 and 2 and 3 and 4). Station (V) completes the rivet connection step between the thin-walled parts (Part1) and the connecting parts (Part4) in subassemblies (Part1 and 2 and 3 and 4) in order to close the

assembly process and form a box-type structure and serves as a measuring station to check the assembly quality and accuracy of the box-type structure. In the actual assembly process, such thin-walled parts with large structural dimensions and weak rigidity usually require the use of a large number of fixtures to constrain their spatial position, often following the “N-2-1” over-positioning principle rather than the “3-2-1” positioning principle. However, the blind use of fixtures is not only ineffective in ensuring the accuracy of the assembled product, but can also cause many problems, such as making the assembly process more redundant and increasing the cost of materials and labor required for assembly. Therefore, this paper still uses the most influential “3-2-1” positioning principle to analyze the assembly deviation of such parts, calculates the deviation of the selected KCC point on the part, combines the spatial triangle penetration detection algorithm, introduces contact penalty force to eliminate the interference and gap between adjacent parts and corrects the position coordinates of the KPC point on the part. Using the sequential change of assembly stations in the assembly process as the time course and the position coordinates of KPC points as the spatial course, the accumulation, flow and transfer of part assembly deviations across multiple assembly stations are revealed to illustrate the deviation transfer mechanism of weakly rigid parts under the “3-2-1” positioning scheme.

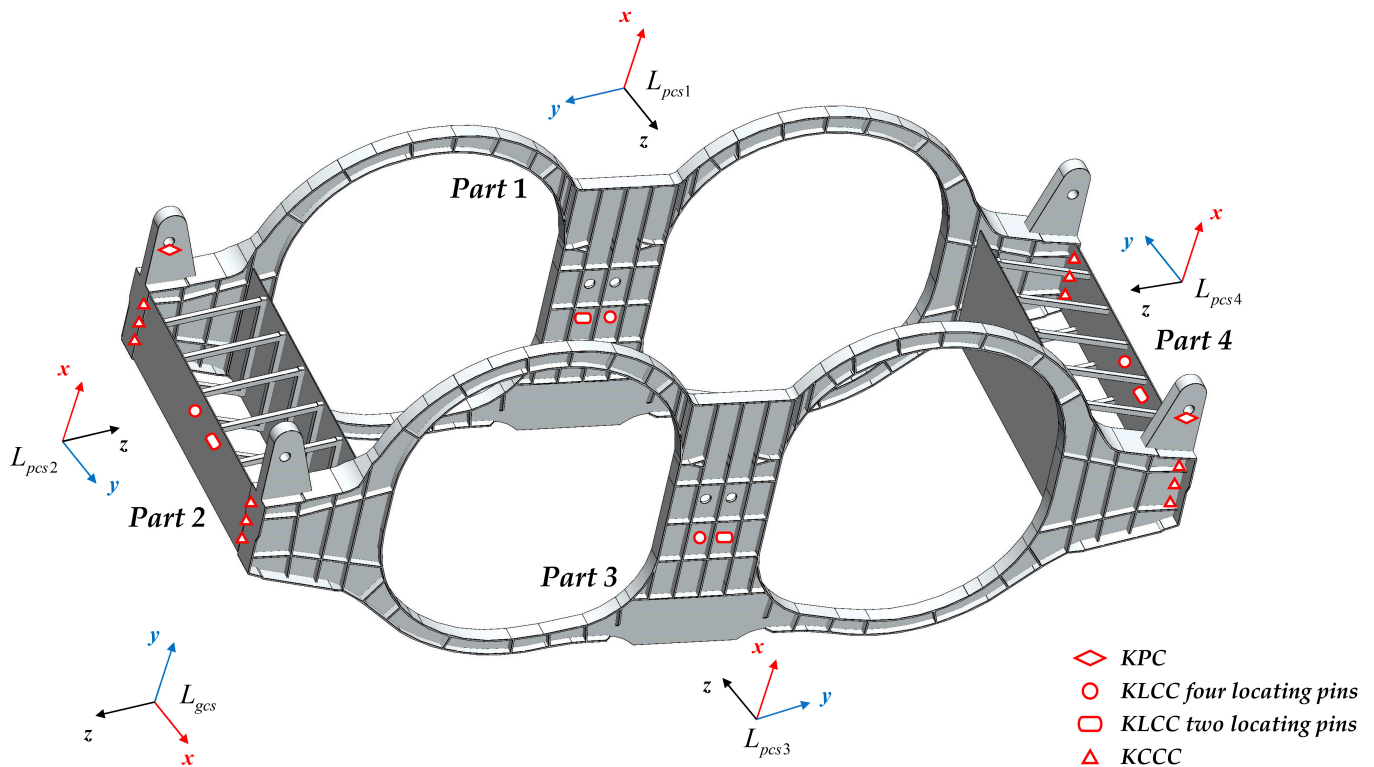


Figure 14. Diagram of the rear fuselage frame structure of the aircraft.

### 7.2. Deviation Transfer Model for MAP

In order to ensure that the assembly deviation transfer mathematical model and the finite element simulation model are year-on-year, it is necessary to specify uniform KPC and KCC points for each part. The deviation of the KLCC point is determined by the fixture manufacturing process. The deviation of KLCC points is determined by processes such as fixture manufacturing, and the deviation of KCCC and KPC points is caused by the flexible deformation of the part. Based on the actual distribution characteristics of KC points on each part and fixture in the deviation source, the initial deviation values of KCCC points on parts Part1 to Part4 in the MAP are obtained, as shown in Table 1.

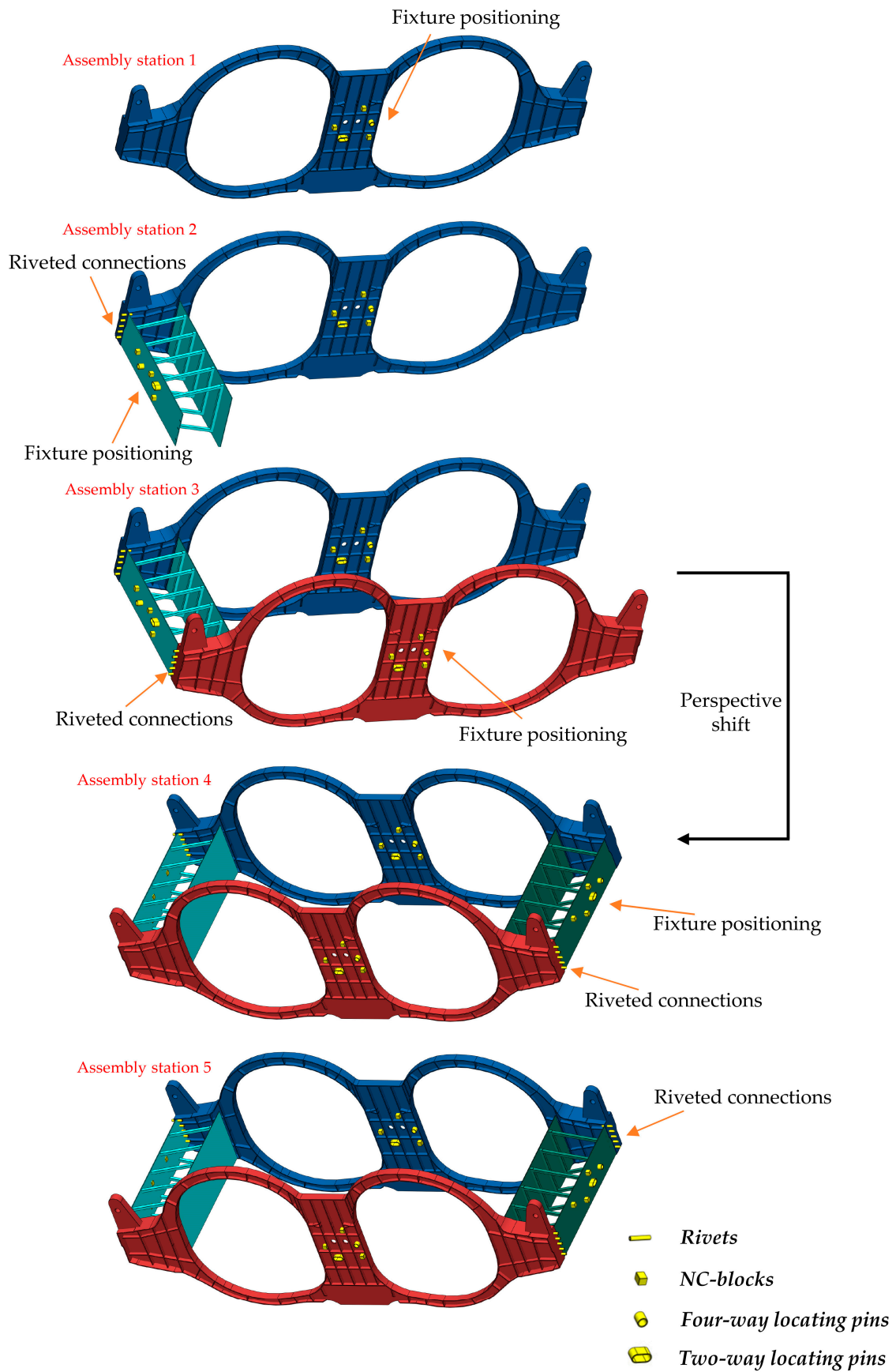


Figure 15. Diagram of the actual assembly production process.

**Table 1.** Deviation value of the KCCC point (flexible deformation already present).

| Part Name | KCCC Point Deviation (x-y-z)/mm <sup>1</sup> |                             |
|-----------|--|-----------------------------|
|           | Contact Fit Zone 1                           | Contact Fit Zone 2          |
| Part 1    | (0, 0, 1.882) (0, 0, 1.882)                  | (0, 0, 2.503) (0, 0, 2.503) |
|           | (0, 0, 1.973) (0, 0, 1.972)                  | (0, 0, 2.556) (0, 0, 2.556) |
| Part 2    | (0, 0, 0) (0, 0, 0)                          | (0, 0, 0) (0, 0, 0)         |
|           | (0, 0, 0) (0, 0, 0)                          | (0, 0, 0) (0, 0, 0)         |
| Part 3    | (0, 0, 1.589) (0, 0, 1.588)                  | (0, 0, 0) (0, 0, 2.121)     |
|           | (0, 0, 1.619) (0, 0, 1.618)                  | (0, 0, 0) (0, 0, 2.183)     |
| Part 4    | (0, 0, 0) (0, 0, 0)                          | (0, 0, 0) (0, 0, 0)         |
|           | (0, 0, 0) (0, 0, 0)                          | (0, 0, 0) (0, 0, 0)         |

<sup>1</sup> Deviation values are counted in the part coordinate system.

Similarly, the initial deviation values of the KLCC points in the MAP were obtained. Due to the flexible deformation of the weakly rigid parts Part1 and Part3 and the influence of the locating pins, the contact action in the contact fit area of each part has a significant non-linear contact phenomenon. In order to control the non-linear contact forces that may cause odd values, the position of the strongly rigid parts Part2 and Part4 is first temporarily adjusted to approximate the fit with Part1 and Part3, assuming an adjustment amount of  $h$ , after ensuring that all four contact pairs have been generated smoothly. Rigid displacement compensation is then applied according to the adjustment amount  $h$  to eliminate gaps and overfills.

Under the part coordinate system shown in Figure 13, the nominal coordinate values of the KPC and KLCC points on the weakly rigid parts Part1 and Part3 and the strongly rigid parts Part2 and Part4 are determined from Table 2 before the assembly process begins.

**Table 2.** Nominal coordinate values of the KLCC point and KPC point in the MAP<sup>1</sup>.

| Part Name | KLCC Point Coordinates <sup>2</sup> |            | KPC Point Coordinates <sup>2</sup> |            |                                |
|-----------|-------------------------------------|------------|------------------------------------|------------|--------------------------------|
|           | KLCC Point Name                     | (x-y-z)/mm | KPC Point Name                     | (x-y-z)/mm |                                |
| Part 1    | Locating pins <sup>3</sup>          | $P_1$      | (−225.763, 1603.796, −23.991)      | $A_1$      | (−76.052, 3357.246, −22.253)   |
|           |                                     | $P_2$      | (−225.797, 1734.796, −24.003)      |            |                                |
| Part 2    | Locating pins <sup>3</sup>          | $P_3$      | (−391.672, 842.316, −3403.190)     | $A_2$      | (−488.994, 253.063, −3403.190) |
|           |                                     | $P_4$      | (−391.638, 511.119, −3403.190)     |            |                                |
| Part 3    | Locating pins <sup>3</sup>          | $P_5$      | (−225.764, −1752.198, −1199.504)   | $A_3$      | (−76.050, 0.646, −1197.504)    |
|           |                                     | $P_6$      | (−225.800, −1603.797, −1199.500)   |            |                                |
| Part 4    | Locating pins <sup>3</sup>          | $P_7$      | (−412.935, −321.565, −46.553)      | $A_4$      | (−319.919, −294.442, −46.5528) |
|           |                                     | $P_8$      | (−419.802, −777.862, −46.5528)     |            |                                |

<sup>1</sup> The data in Table 2 already existed when the flexible deformation of the parts was counted. <sup>2</sup> Deviation values are counted in the part coordinate system. <sup>3</sup> Locating pins indicate four-way locating pins and two-way locating pins; there are four parts in the case, so there are four four-way locating pins and four two-way locating pins.

According to Tables 1 and 2, the spatial postures of parts Part1 to Part4 are determined, and the system matrices  $B$ ,  $E$ ,  $F$ ,  $G$  and  $L$  in the MAP are calculated to obtain the posture of each part under the coupling effect of its own flexible deformation and fixture positioning deviation. The coordinates of the KCCC points in the contact and fit area are obtained to reconstruct the contact state between the parts in the contact and fit area. The flush transformation matrix of parts Part1 to Part4 are calculated from the part coordinate system  $L_{pcs \times}$  ( $x = 1, 2, 3, 4$ ) to  $L_{gcs}$ , respectively, and MATLAB 9.10 software is used to implement the spatial triangle intersection detection algorithm and the spatial triangle penetration detection algorithm based on the deviation of the part measurement points to apply penalty force to the contact fit surface of each part to correct the contact gap or penetration. Finally, the mathematical modelling of the assembly deviation transfer model of each part in the

above frame structure is completed and the state space equation for the multi-level assembly deviation transfer of the frame structure is obtained according to Equations (43)–(45):

$$X(k) = X(k - 1) + D^P(k) + D^Q(k) + R(k) \tag{43}$$

$$D^P(k) = B(k) \cdot U(k) = L(k) \cdot E(k) \cdot F(k) \cdot G(k) \cdot U(k) \tag{44}$$

$$D^Q(k) = S(k) \cdot C(k) \cdot T(k) \tag{45}$$

In Equations (43)–(45),  $k = 1, 2, 3, 4, 5$ . The specific values of the system matrices  $E, F, G$  and  $L$  in this mathematical model are:

$$E(1) = \begin{bmatrix} E_{A_1,P_1} & 0^{5 \times 15} \\ 0^{15 \times 1} & 0^{15 \times 15} \end{bmatrix}, E(2) = \begin{bmatrix} E_{A_1,P_1} & 0^{5 \times 5} & 0 \\ 0^{5 \times 5} & E_{A_2,P_3} & \vdots \\ 0 & \dots & 0^{10 \times 10} \end{bmatrix}, E(3) = \begin{bmatrix} E_{A_1,P_1} & 0^{5 \times 5} & 0^{5 \times 5} & 0 \\ 0^{5 \times 5} & E_{A_2,P_3} & 0^{5 \times 5} & \vdots \\ 0^{5 \times 5} & 0^{5 \times 5} & E_{A_3,P_5} & \vdots \\ 0 & \dots & \dots & 0^{5 \times 5} \end{bmatrix} \tag{46}$$

$$E(4) = \begin{bmatrix} E_{A_1,P_1} & 0^{5 \times 5} & 0^{5 \times 5} & 0^{5 \times 5} \\ 0^{5 \times 5} & E_{A_2,P_3} & 0^{5 \times 5} & 0^{5 \times 5} \\ 0^{5 \times 5} & 0^{5 \times 5} & E_{A_3,P_5} & 0^{5 \times 5} \\ 0^{5 \times 5} & 0^{5 \times 5} & 0^{5 \times 5} & E_{A_4,P_7} \end{bmatrix}, E(5) = \begin{bmatrix} E_{A_1,P_1} & 0^{5 \times 5} & 0^{5 \times 5} & 0^{5 \times 5} \\ 0^{5 \times 5} & E_{A_2,P_3} & 0^{5 \times 5} & 0^{5 \times 5} \\ 0^{5 \times 5} & 0^{5 \times 5} & E_{A_3,P_5} & 0^{5 \times 5} \\ 0^{5 \times 5} & 0^{5 \times 5} & 0^{5 \times 5} & E_{A_4,P_7} \end{bmatrix}$$

$$E_{A_1,P_1} = \begin{bmatrix} 1 & 0 & 0 & 1753 & 0 \\ 0 & 1 & 0 & -149 & 0 \\ 0 & 0 & 1 & 0 & 1753 \\ 0 & 0 & 0 & 1 & 0 \\ 0 & 0 & 0 & 0 & 1 \end{bmatrix}, E_{A_2,P_3} = \begin{bmatrix} 1 & 0 & 0 & 589 & 0 \\ 0 & 1 & 0 & -97 & 0 \\ 0 & 0 & 1 & 0 & 589 \\ 0 & 0 & 0 & 1 & 0 \\ 0 & 0 & 0 & 0 & 1 \end{bmatrix} \tag{47}$$

$$E_{A_3,P_5} = \begin{bmatrix} 1 & 0 & 0 & 1752 & 0 \\ 0 & 1 & 0 & -149 & 0 \\ 0 & 0 & 1 & 0 & 1752 \\ 0 & 0 & 0 & 1 & 0 \\ 0 & 0 & 0 & 0 & 1 \end{bmatrix}, E_{A_4,P_7} = \begin{bmatrix} 1 & 0 & 0 & 27 & 0 \\ 0 & 1 & 0 & -21 & 0 \\ 0 & 0 & 1 & 0 & 27 \\ 0 & 0 & 0 & 1 & 0 \\ 0 & 0 & 0 & 0 & 1 \end{bmatrix}$$

$$F(1) = \begin{bmatrix} F_{A_1,P_1} & 0^{5 \times 15} \\ 0^{15 \times 5} & 0^{15 \times 15} \end{bmatrix}, F(2) = \begin{bmatrix} F_{A_1,P_1} & 0^{5 \times 5} & 0 \\ 0^{5 \times 5} & F_{A_2,P_3} & \vdots \\ 0 & \dots & 0^{10 \times 10} \end{bmatrix}, F(3) = \begin{bmatrix} F_{A_1,P_1} & 0^{5 \times 5} & 0^{5 \times 5} & 0 \\ 0^{5 \times 5} & F_{A_2,P_3} & 0^{5 \times 5} & \vdots \\ 0^{5 \times 5} & 0^{5 \times 5} & F_{A_3,P_5} & \vdots \\ 0 & \dots & \dots & 0^{5 \times 5} \end{bmatrix} \tag{48}$$

$$F(4) = \begin{bmatrix} F_{A_1,P_1} & 0^{5 \times 5} & 0^{5 \times 5} & 0^{5 \times 5} \\ 0^{5 \times 5} & F_{A_2,P_3} & 0^{5 \times 5} & 0^{5 \times 5} \\ 0^{5 \times 5} & 0^{5 \times 5} & F_{A_3,P_5} & 0^{5 \times 5} \\ 0^{5 \times 5} & 0^{5 \times 5} & 0^{5 \times 5} & F_{A_4,P_7} \end{bmatrix}, F(5) = \begin{bmatrix} F_{A_1,P_1} & 0^{5 \times 5} & 0^{5 \times 5} & 0^{5 \times 5} \\ 0^{5 \times 5} & F_{A_2,P_3} & 0^{5 \times 5} & 0^{5 \times 5} \\ 0^{5 \times 5} & 0^{5 \times 5} & F_{A_3,P_5} & 0^{5 \times 5} \\ 0^{5 \times 5} & 0^{5 \times 5} & 0^{5 \times 5} & F_{A_4,P_7} \end{bmatrix}$$

$$F_{A_1,P_1} = \begin{bmatrix} 1 & 0 & 0 & 0 & 0 \\ 0 & 1 & 0 & 0 & 0 \\ 0 & 0 & 1 & 0 & 0 \\ 0 & 0 & 0 & 1 & 0 \\ 0 & 0 & 0 & 0 & -11 \end{bmatrix}, F_{A_2,P_3} = \begin{bmatrix} 1 & 0 & 0 & 0 & 0 \\ 0 & 1 & 0 & 0 & 0 \\ 0 & 0 & 1 & 0 & 0 \\ 0 & 0 & 0 & 1 & 0 \\ 0 & 0 & 0 & 0 & NaN \end{bmatrix} \tag{49}$$

$$F_{A_3,P_5} = \begin{bmatrix} 1 & 0 & 0 & 0 & 0 \\ 0 & 1 & 0 & 0 & 0 \\ 0 & 0 & 1 & 0 & 0 \\ 0 & 0 & 0 & 1 & 0 \\ 0 & 0 & 0 & 0 & 51 \end{bmatrix}, F_{A_4,P_7} = \begin{bmatrix} 1 & 0 & 0 & 0 & 0 \\ 0 & 1 & 0 & 0 & 0 \\ 0 & 0 & 1 & 0 & 0 \\ 0 & 0 & 0 & 1 & 0 \\ 0 & 0 & 0 & 0 & NaN \end{bmatrix}$$

$$\begin{aligned}
 G(1) &= \begin{bmatrix} G_{P_1,P_2} & 0^{5 \times 18} \\ 0^{15 \times 6} & 0^{15 \times 18} \end{bmatrix}, G(2) = \begin{bmatrix} G_{P_1,P_2} & 0^{5 \times 6} & 0 \\ 0^{5 \times 6} & G_{P_3,P_4} & \vdots \\ 0 & \dots & 0^{10 \times 12} \end{bmatrix}, G(3) = \begin{bmatrix} G_{P_1,P_2} & 0^{5 \times 6} & 0^{5 \times 6} & 0 \\ 0^{5 \times 6} & G_{P_3,P_4} & 0^{5 \times 6} & \vdots \\ 0^{5 \times 6} & 0^{5 \times 5} & G_{P_5,P_6} & \\ 0 & \dots & & 0^{5 \times 6} \end{bmatrix} \\
 G(4) &= \begin{bmatrix} G_{P_1,P_2} & 0^{5 \times 6} & 0^{5 \times 6} & 0^{5 \times 6} \\ 0^{5 \times 6} & G_{P_3,P_4} & 0^{5 \times 6} & 0^{5 \times 6} \\ 0^{5 \times 6} & 0^{5 \times 5} & G_{P_5,P_6} & 0^{5 \times 6} \\ 0^{5 \times 6} & 0^{5 \times 6} & 0^{5 \times 6} & G_{P_7,P_8} \end{bmatrix}, G(5) = \begin{bmatrix} F_{A_1,P_1} & 0^{5 \times 5} & 0^{5 \times 5} & 0^{5 \times 5} \\ 0^{5 \times 5} & F_{A_2,P_3} & 0^{5 \times 5} & 0^{5 \times 5} \\ 0^{5 \times 5} & 0^{5 \times 5} & F_{A_3,P_5} & 0^{5 \times 5} \\ 0 & 0^{5 \times 5} & 0^{5 \times 5} & F_{A_4,P_7} \end{bmatrix}
 \end{aligned} \tag{50}$$

$$\begin{aligned}
 G_{P_1,P_2} &= \begin{bmatrix} 1 & 0 & 0 & 0 & 0 & 0 \\ 0 & 1 & 0 & 0 & 0 & 0 \\ 0 & 0 & 1 & 0 & 0 & 0 \\ -0.0076 & 0 & 0 & 0.0076 & 0 & 0 \\ 0 & 0 & -0.0076 & 0 & 0 & 0.0076 \end{bmatrix}, G_{P_3,P_4} = \begin{bmatrix} 1 & 0 & 0 & 0 & 0 & 0 \\ 0 & 1 & 0 & 0 & 0 & 0 \\ 0 & 0 & 1 & 0 & 0 & 0 \\ -0.0030 & 0 & 0 & 0.0030 & 0 & 0 \\ 0 & 0 & -0.0030 & 0 & 0 & 0.0030 \end{bmatrix} \\
 G_{P_5,P_6} &= \begin{bmatrix} 1 & 0 & 0 & 0 & 0 & 0 \\ 0 & 1 & 0 & 0 & 0 & 0 \\ 0 & 0 & 1 & 0 & 0 & 0 \\ -0.0067 & 0 & 0 & 0.0067 & 0 & 0 \\ 0 & 0 & -0.0067 & 0 & 0 & 0.0067 \end{bmatrix}, G_{P_7,P_8} = \begin{bmatrix} 1 & 0 & 0 & 0 & 0 & 0 \\ 0 & 1 & 0 & 0 & 0 & 0 \\ 0 & 0 & 1 & 0 & 0 & 0 \\ -0.0022 & 0 & 0 & 0.0022 & 0 & 0 \\ 0 & 0 & -0.0022 & 0 & 0 & 0.0022 \end{bmatrix}
 \end{aligned} \tag{51}$$

$$\begin{aligned}
 L(1) &= [0^{20 \times 20}], L(2) = \begin{bmatrix} \Pi_1 & 0^{5 \times 15} \\ 0^{15 \times 5} & 0^{15 \times 15} \end{bmatrix}, L(3) = \begin{bmatrix} \Pi_1 & 0^{5 \times 5} & 0 \\ 0^{5 \times 5} & \Pi_2 & \vdots \\ 0 & \dots & 0^{5 \times 5} \end{bmatrix} \\
 L(4) &= \begin{bmatrix} \Pi_1 & 0^{5 \times 5} & 0^{5 \times 5} & 0 \\ 0^{5 \times 5} & \Pi_2 & 0^{5 \times 5} & \vdots \\ 0^{5 \times 5} & 0^{5 \times 5} & \Pi_3 & 0^{5 \times 5} \\ 0 & \dots & & 0^{5 \times 5} \end{bmatrix}, L(5) = \begin{bmatrix} \Pi_1 & 0^{5 \times 5} & 0^{5 \times 5} & 0 \\ 0^{5 \times 5} & \Pi_2 & 0^{5 \times 5} & 0^{5 \times 5} \\ 0^{5 \times 5} & 0^{5 \times 5} & \Pi_3 & 0^{5 \times 5} \\ 0^{5 \times 5} & 0^{5 \times 5} & 0^{5 \times 5} & \Pi_4 \end{bmatrix}
 \end{aligned} \tag{52}$$

$$\Pi_1 = \begin{bmatrix} 0 & 0 & 1 \\ 1 & 0 & 0 \\ 0 & 1 & 0 \end{bmatrix}, \Pi_2 = \begin{bmatrix} 0 & 1 & 0 \\ 1 & 0 & 0 \\ 0 & 0 & -1 \end{bmatrix}, \Pi_3 = \begin{bmatrix} 0 & 0 & -1 \\ 1 & 0 & 0 \\ 0 & -1 & 0 \end{bmatrix}, \Pi_4 = \begin{bmatrix} 0 & -1 & 0 \\ 1 & 0 & 0 \\ 0 & 0 & 1 \end{bmatrix} \tag{53}$$

Based on the actual assembly process in this case, assembly simulation tests were carried out to verify the validity of the mathematical model for assembly deviation transfer. Based on the KLCC point deviation values described in Table 3, a finite element simulation model of the assembly process for the frame-shaped structure was created in Abaqus 2021 software. In order to avoid penetrations between parts and components in areas that do not conform to the laws of physics, four contact pairs are defined in the assembly process of the frame-shaped structure. In the positioning phase, the geometry of fixture elements, such as positioning blocks, slots, holes and pins, is much smaller than the geometry of the part or subassembly, so the geometric features of the fixture elements are ignored and the geometric contact between the fixture elements and the part or subassembly is simplified. Based on the fixture layout data from the actual assembly process, boundary constraints are applied to the part or subassembly in the form of points. In order to exclude the influence of mesh size and unreasonable element type on the test results, and to comprehensively consider the geometric complexity of each part in the case, it is decided to use the C3D10M element type. The C3D10M element uses the form function with linear interpolation to approximate its internal variables. This makes it suitable for simulating linear elastic and plastic behavior over small strain ranges. In addition, the model response with a mesh size of 10–30 mm was tested to analyze the mesh convergence. In this mesh size range, the mesh size has little influence on the simulation results, so it is logical to think that the mesh size is not sensitive to the simulation results. In the rivet fastening phase, the contact action in the contact fit area of each part is significantly non-linear due to the flexible deformation

of the weakly rigid parts Part1 and Part3 and the influence of the locating pins. The four sliding friction contact pairs are defined and the strong rigid parts Part2 and Part4 are first temporarily adjusted to approximate the fit with Part1 and Part3 to ensure that all four contact pairs have been created smoothly, and then the deviation of the locating blocks in Table 3 is considered as rigid displacement to eliminate the gap and overfill to achieve a tight fit in the contact area. Subsequently, the four defined sliding contact pairs are modified to bound contact to simulate the rigid connection between the parts (subassemblies) after riveting. The simulation results for the frame structure MAP are shown in the deviation deformation cloud map (unit: mm) in Figure 16.

Table 3. Deviation value of the KLCC point.

| Part Name | KLCC Point Deviation <sup>1</sup> |                |        |       |        |
|-----------|-----------------------------------|----------------|--------|-------|--------|
|           | KLCC Point Name                   |                | x/mm   | y/mm  | z/mm   |
| Part 1    | Locating pins <sup>2</sup>        | P <sub>1</sub> | 0.100  | 0.100 | —      |
|           |                                   | P <sub>2</sub> | 0.050  | —     | —      |
|           | Locating blocks <sup>3</sup>      |                | —      | —     | —      |
| Part 2    | Locating pins                     | P <sub>3</sub> | 0      | 0     | —      |
|           | Locating blocks                   | P <sub>4</sub> | 0      | —     | —      |
| Part 3    | Locating pins                     | P <sub>5</sub> | 0.050  | 0.100 | —      |
|           |                                   | P <sub>6</sub> | −0.050 | —     | —      |
|           | Locating blocks                   |                | —      | —     | —      |
| Part 4    | Locating pins                     | P <sub>7</sub> | 0      | 0     | —      |
|           | Locating blocks                   | P <sub>8</sub> | 0      | —     | —      |
|           |                                   |                | —      | —     | −0.150 |

<sup>1</sup> Deviation values are counted in the part coordinate system. <sup>2</sup> Locating pins indicate four-way locating pins and two-way locating pins; there are four parts in the case, so there are four four-way locating pins and four two-way locating pins. <sup>3</sup> Locating blocks are NC blocks, in which case the error of the locating blocks is ignored and their deviation in the z direction in Table 3 is equal to the rigid displacement compensation h.

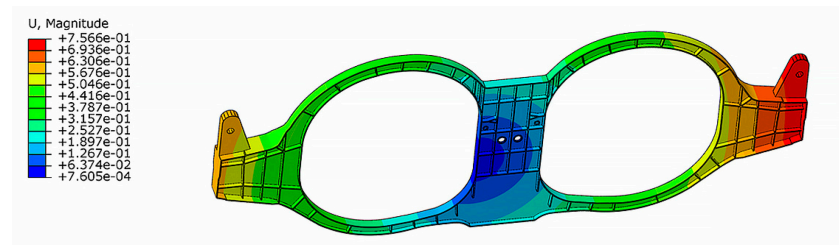


Figure 16. Cont.

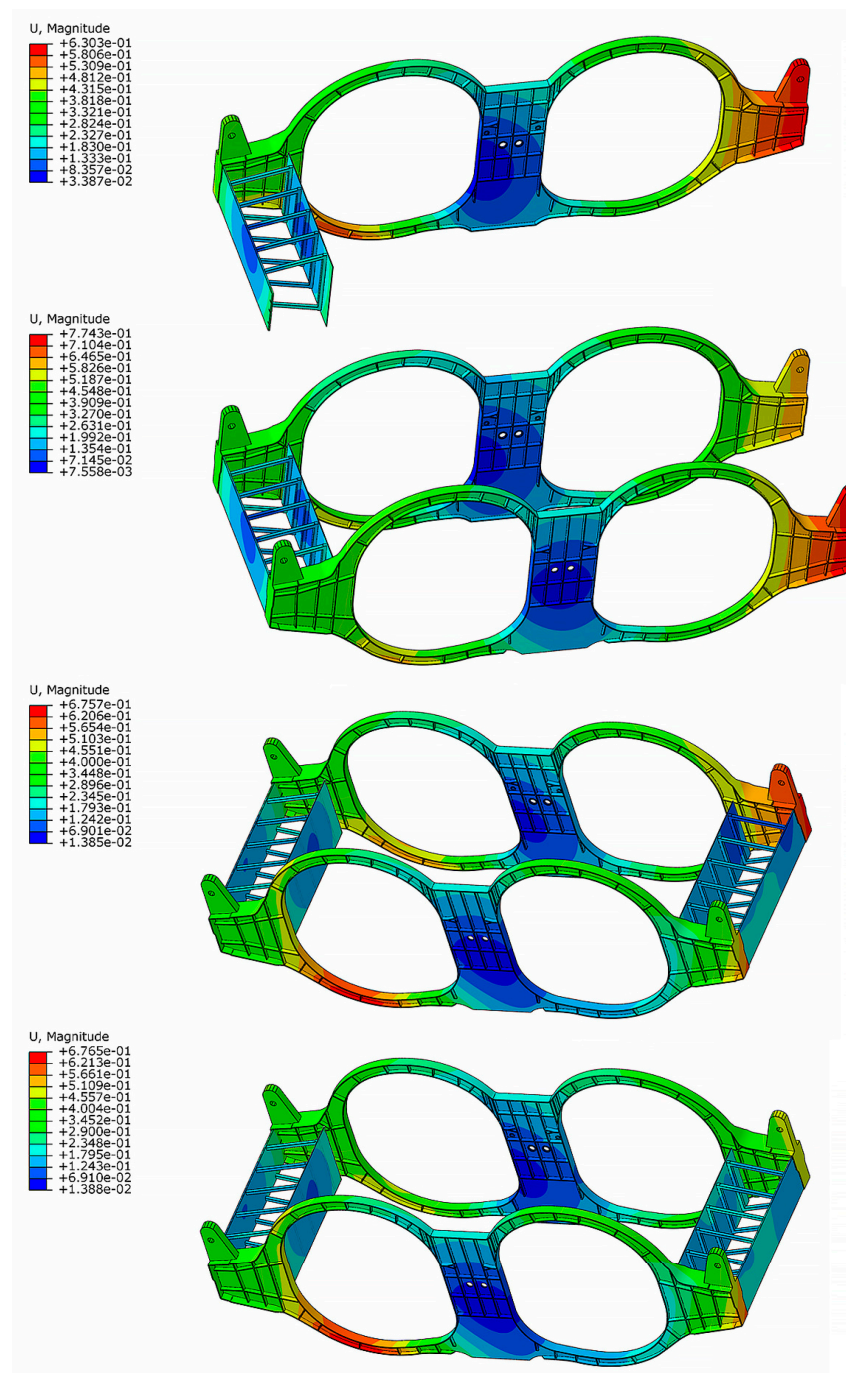
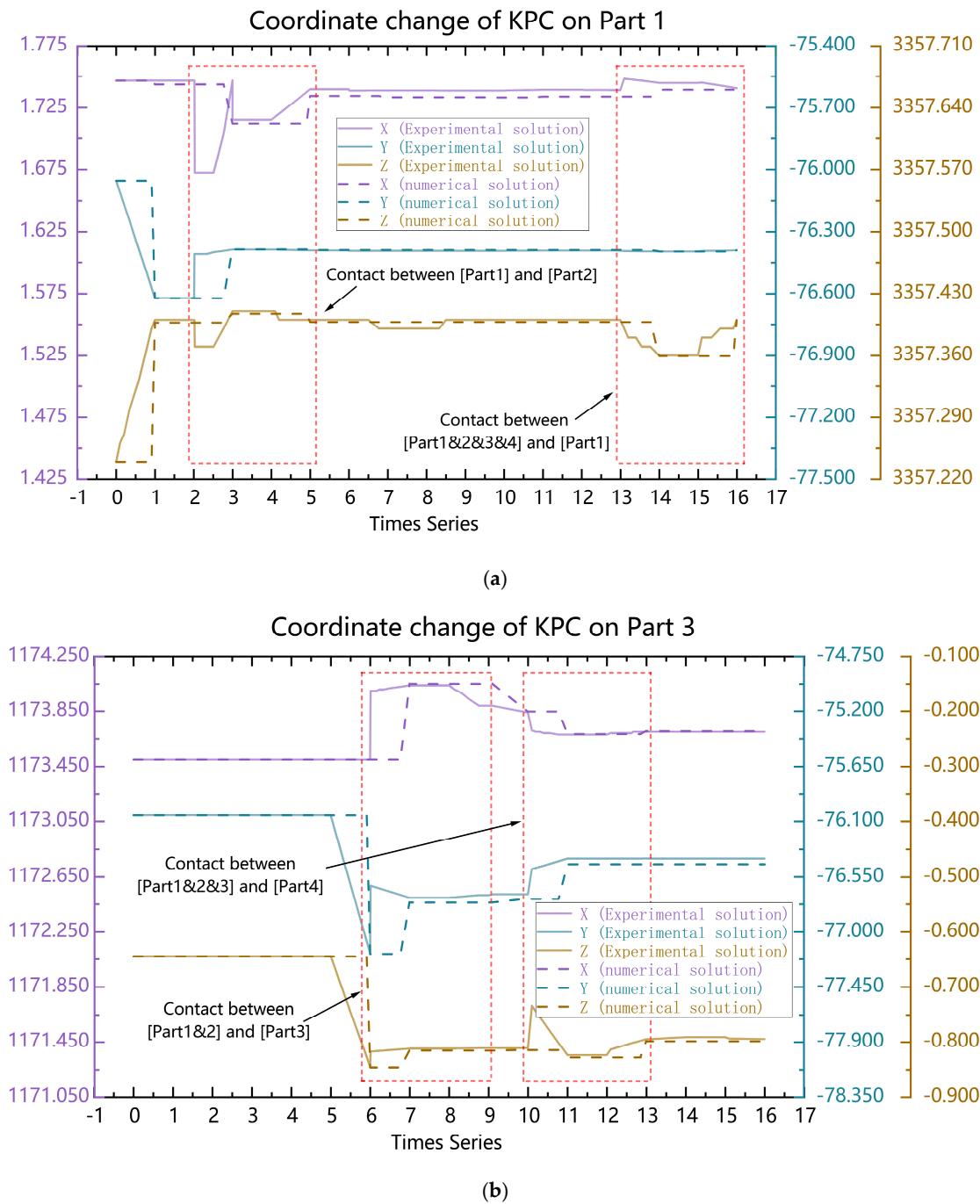


Figure 16. Deviation cloud for a MAP finite element simulation of frame structure.

## 8. Results

In the MAP of the frame structure, there are four KPC points; however, since the parts Part2 and Part4 do not have their own flexible deformation and fixture positioning deviation, the deviation of their KPC points is not recorded, and the change of the coordinates of the KPC points calculated by the mathematical model of assembly deviation transfer and the finite element simulation test can be seen in Figure 17. The results of the assembly deviations of the two techniques are compared, the former being the calculated values and the latter being the theoretical values. The difference between the calculated and the theoretical values is not significant throughout the time series, with the error between the two remaining within 15%.



**Figure 17.** Deviation prediction results and simulation results of KPC points in the MAP frame structure as: (a) Coordinate change of KPC on Part1. (b) Coordinate change of KPC on Part3.

### 9. Discussion and Conclusions

The growing number of stations and parts in the multi-station thin plate assembly process contributes to the increased complexity of the deviation flow. Ensuring the dimensional accuracy of the product necessitates not only controlling the dimensional deviation of the final product, but also monitoring the deviation flow throughout the assembly process. The state space model offers the mathematical foundation for detecting and controlling dimensional deviation flow.

The escalation in the number and variety of parts involved in multi-station part assembly contributes to the increased intricacy of the deviation flow’s variation. Product quality hinges not only on the dimensional deviation of the end product, but also on the capability

to monitor the origin, transformation, accumulation and transmission of the deviation flow during assembly. First, a state space model for multi-station part assembly is formulated, designed to track the variation of KPC points at each assembly stage. Subsequently, three categories of bias sources—part manufacturing bias, fixture positioning bias and assembly contact bias—associated with product and process characteristics are accounted for. The accuracy of the proposed deviation transfer model in this paper is validated through a real-life example from the aerospace manufacturing sector. The advantages of this deviation transfer model encompass the following.

1. Based on the existence of flexible deformation in weakly rigid parts, the manufacturing deviations and fixture positioning deviations of parts are decomposed into rigid deviations in typical part dimensional planes and flexible deviations in atypical part dimensional planes, and assembled into a coefficient matrix, which is convenient for machine coding and secondary development.
2. The proposed deviation transfer model takes into account the influence of assembly contact forces on part deviations in the assembly process, making it more valuable for practical applications than previous deviation flow models.
3. The model can be applied not only in aerospace manufacturing, but also within multi-level assembly production industries containing weakly rigid plate and beam parts, such as automotive manufacturing and ship manufacturing, contributing to promising applications in upstream parts.

**Author Contributions:** The authors' contributions are as follows X.H. and Y.Z. were responsible for the design and operation of the whole experiment; X.H. wrote the manuscript; M.W. made a lot of constructive suggestions regarding the test ideas and assisted in analyzing the test data; P.H. provided assistance for the finite element simulation experiments. All authors have read and agreed to the published version of the manuscript.

**Funding:** This research was supported by the Applied Basic Research Program of the Department of Science and Technology of Liaoning Province, China (2022JH2/101300213) and the National Natural Science Foundation of China (51875367).

**Institutional Review Board Statement:** Not applicable.

**Informed Consent Statement:** Not applicable.

**Data Availability Statement:** The data presented in this study are available on request from the corresponding author. The data are not publicly available due to privacy.

**Conflicts of Interest:** The authors declare no conflict of interest.

## References

1. Takezawa, N. An Improved Method for Establishing the Process-Wise Quality Standard. *Rep. Stat. Appl. Res. Union. Jpn. Sci. Eng.* **1980**, *27*, 63–75.
2. Liu, S.C.; Hu, S.J. Variation Simulation for Deformable Sheet Metal Assemblies Using Finite Element Methods. *J. Manuf. Sci. Eng.* **1997**, *119*, 368–374. [[CrossRef](#)]
3. Liu, S.C.; Hu, S.J. Sheet Metal Joint Configurations and Their Variation Characteristics. *J. Manuf. Sci. Eng.* **1998**, *120*, 461–467. [[CrossRef](#)]
4. Cai, N.; Qiao, L. Rigid-Compliant Hybrid Variation Modeling of Sheet Metal Assembly with 3D Generic Free Surface. *J. Manuf. Syst.* **2016**, *41*, 45–64. [[CrossRef](#)]
5. Qu, X.; Li, X.; Ma, Q.; Wang, X. Variation Propagation Modeling for Locating Datum System Design in Multi-Station Assembly Processes. *Int. J. Adv. Manuf. Tech.* **2016**, *86*, 1357–1366. [[CrossRef](#)]
6. Jandaghi Shahi, V.; Masoumi, A. Integration of In-Plane and out-of-Plane Dimensional Variation in Multi-Station Assembly Process for Automotive Body Assembly. *Proc. Inst. Mech. Eng. Part D J. Automob. Eng.* **2020**, *234*, 1690–1702. [[CrossRef](#)]
7. Liu, Y.; Sun, R.; Lu, Y.; Zhang, S. A Knowledge-Based Online Fault Detection Method of the Assembly Process Considering the Relative Poses of Components. *Int. J. Precis. Eng. Man.* **2019**, *20*, 1705–1720. [[CrossRef](#)]
8. Dahlström, S.; Lindkvist, L. Variation Simulation of Sheet Metal Assemblies Using the Method of Influence Coefficients with Contact Modeling. *J. Manuf. Sci. Eng.* **2006**, *129*, 615–622. [[CrossRef](#)]
9. Jin, S.; Ding, S.; Li, Z.; Yang, F.; Ma, X. Point-Based Solution Using Jacobian-Torsor Theory into Partial Parallel Chains for Revolving Components Assembly. *J. Manuf. Syst.* **2018**, *46*, 46–58. [[CrossRef](#)]

10. Zhang, M.; Liu, Y.; Wang, D.; Tan, J. A Coaxiality Measurement Method for the Aero-Engine Rotor Based on Common Datum Axis. *Measurement* **2022**, *191*, 110696. [[CrossRef](#)]
11. Yu, H.; Zhao, C.; Lai, X. Compliant Assembly Variation Analysis of Scalloped Segment Plates with a New Irregular Quadrilateral Plate Element Via ANCF. *J. Manuf. Sci. Eng.* **2018**, *140*, 091006. [[CrossRef](#)]
12. Ramesh Sagar, V.; Wärmefjord, K.; Söderberg, R. Effect of Selective Laser Heat Treatment on Geometrical Variation in Boron Steel Components: An Experimental Investigation. *Proc. Inst. Mech. Eng. Part B J. Eng. Manuf.* **2021**, *235*, 54–64. [[CrossRef](#)]
13. Zhang, J.; Qiao, L.; Huang, Z.; Anwer, N. Point-by-Point-Contact-Based Approach to Compute Position and Orientation between Parts Assembled by Multiple Non-Ideal Planes. *Appl. Sci.* **2022**, *12*, 1596. [[CrossRef](#)]
14. Xie, K.; Wells, L.; Camelio, J.A.; Youn, B.D. Variation Propagation Analysis on Compliant Assemblies Considering Contact Interaction. *J. Manuf. Sci. Eng.* **2007**, *129*, 934–942. [[CrossRef](#)]
15. Khader, M. Hamdia, Hamid Ghasemi. Reliability analysis of the stress intensity factor using multilevel Monte Carlo methods. *Probabilist Eng. Mech.* **2023**, *74*, 103497. [[CrossRef](#)]
16. Xi, Y.; Gao, Z.; Chen, K.; Dai, H.; Liu, Z. Error Propagation Model Using Jacobian-Torsor Model Weighting for Assembly Quality Analysis on Complex Product. *Mathematics* **2022**, *10*, 3534. [[CrossRef](#)]
17. Laperrrière, L.; ElMaraghy, H.A. Tolerance Analysis and Synthesis Using Jacobian Transforms. *CIRP Annals* **2000**, *49*, 359–362. [[CrossRef](#)]
18. Chen, H.; Jin, S.; Li, Z.; Lai, X. A Solution of Partial Parallel Connections for the Unified Jacobian–Torsor Model. *Mech. Mach. Theory* **2015**, *91*, 39–49. [[CrossRef](#)]
19. Liu, T.; Zhao, Q.; Cao, Y.; Yang, J. A Generic Approach for Analysis of Mechanical Assembly. *Precis. Eng.* **2018**, *54*, 361–370. [[CrossRef](#)]
20. Liu, S.C.; Hu, S.J.; Woo, T.C. Tolerance Analysis for Sheet Metal Assemblies. *J. Mech. Design* **1996**, *118*, 62–67. [[CrossRef](#)]
21. Jin, J.; Shi, J. State Space Modeling of Sheet Metal Assembly for Dimensional Control. *J. Manuf. Sci. Eng.* **1999**, *121*, 756–762. [[CrossRef](#)]
22. Mantripragada, R.; Whitney, D.E. Modeling and Controlling Variation Propagation in Mechanical Assemblies Using State Transition Models. *IEEE Trans. Robot. Autom.* **1999**, *15*, 124–140. [[CrossRef](#)]
23. Camelio, J.; Hu, S.J.; Ceglarek, D. Modeling Variation Propagation of Multi-Station Assembly Systems with Compliant Parts. *J. Mech. Design* **2004**, *125*, 673–681. [[CrossRef](#)]
24. Qiu, H.; Feng, Y.; Hong, Z.; Li, K.; Tan, J. Privacy-Preserving for Assembly Deviation Prediction in a Machine Learning Model of Hydraulic Equipment under Value Chain Collaboration. *Sci. Rep.* **2022**, *12*, 10733. [[CrossRef](#)] [[PubMed](#)]
25. Mu, X.; Wang, Y.; Yuan, B.; Sun, W.; Liu, C.; Sun, Q. A New Assembly Precision Prediction Method of Aeroengine High-Pressure Rotor System Considering Manufacturing Error and Deformation of Parts. *J. Mech. Des.* **2021**, *61*, 112–124. [[CrossRef](#)]
26. Masoumi, A.; Shahi, V.J. Fixture Layout Optimization in Multi-Station Sheet Metal Assembly Considering Assembly Sequence and Datum Scheme. *Int. J. Adv. Manuf. Tech.* **2018**, *95*, 4629–4643. [[CrossRef](#)]
27. He, G.; Guo, L.; Li, S.; Zhang, D. Simulation and Analysis for Accuracy Prediction and Adjustment for Machine Tool Assembly Process. *Adv. Mech. Eng.* **2017**, *9*, 168781401773447. [[CrossRef](#)]

**Disclaimer/Publisher’s Note:** The statements, opinions and data contained in all publications are solely those of the individual author(s) and contributor(s) and not of MDPI and/or the editor(s). MDPI and/or the editor(s) disclaim responsibility for any injury to people or property resulting from any ideas, methods, instructions or products referred to in the content.